

Developmental Mechanisms Linking Form and Function During Jaw Evolution

Authors: Katherine C. Woronowicz, Stephanie E. Gline, Safa T. Herfat, Aaron J. Fields, and Richard A. Schneider*

Affiliations: Department of Orthopaedic Surgery, University of California, San Francisco, San Francisco, CA, 94143

***Correspondence to:**

Richard A. Schneider

University of California, San Francisco

Department of Orthopaedic Surgery

513 Parnassus Avenue

S-1164, Box 0514

San Francisco, CA 94143-0514

rich.schneider@ucsf.edu

[Phone: 415-502-3788](tel:415-502-3788)

1 **Abstract**

2 How does form arise during development and change during evolution? How does form
3 relate to function, and what enables embryonic structures to presage their later use in
4 adults? To address these questions, we leverage the distinct functional morphology of
5 the jaw in duck, chick, and quail. In connection with their specialized mode of feeding,
6 duck develop a secondary cartilage at the tendon insertion of their jaw adductor muscle
7 on the mandible. An equivalent cartilage is absent in chick and quail. We hypothesize
8 that species-specific jaw architecture and mechanical forces promote secondary
9 cartilage in duck through the differential regulation of FGF and TGF β signaling. First, we
10 perform transplants between chick and duck embryos and demonstrate that the ability
11 of neural crest mesenchyme (NCM) to direct the species-specific insertion of muscle
12 and the formation of secondary cartilage depends upon the amount and spatial
13 distribution of NCM-derived connective tissues. Second, we quantify motility and build
14 finite element models of the jaw complex in duck and quail, which reveals a link
15 between species-specific jaw architecture and the predicted mechanical force
16 environment. Third, we investigate the extent to which mechanical load mediates FGF
17 and TGF β signaling in the duck jaw adductor insertion, and discover that both pathways
18 are mechano-responsive and required for secondary cartilage formation. Additionally,
19 we find that FGF and TGF β signaling can also induce secondary cartilage in the
20 absence of mechanical force or in the adductor insertion of quail embryos. Thus, our
21 results provide novel insights on molecular, cellular, and biomechanical mechanisms
22 that couple musculoskeletal form and function during development and evolution.

23

24 **Introduction**

25 One of the most remarkable aspects of being an embryo, and a phenomenon that has
26 intrigued embryologists since Aristotle, is the ability to grow in a manner “rather
27 prospective than retrospective” (Thompson, 1942). In theory, how the form of an
28 embryo can presage later adult function is explained by Aristotle’s observation that “the
29 organism is the $\tau\epsilon\lambda\omicron\varsigma$, or final cause, of its own process of generation and development”
30 (Thompson, 1942). But elucidating precise molecular mechanisms that link form and
31 function, and specifically whether form arises from function or function follows form
32 remains challenging, because, like the chicken and the egg, form and function are
33 seamlessly intertwined during development and evolution.

34

35 Some of the most illustrious instances of form and function appear in the craniofacial
36 complex in birds, which are masters of adaptation. A specialized beak seems to exist for
37 every avian diet: insectivore, granivore, nectarivore, frugivore, carnivore, omnivore, etc.
38 (Schneider, 2007; Zusi, 1993). Each diet is supported by a range of structural
39 adaptations to the jaw including size, shape, and sites of muscle attachments (Fish and
40 Schneider, 2014b; Tokita and Schneider, 2009). For example, in *Anseriformes*, or
41 waterfowl such as duck, which use their broad bills to dredge sediment for food, the
42 mandibular adductor (MA) muscle attaches laterally to a large protruding coronoid
43 process (CP) on the mandible. Such a configuration provides a robust insertion site for
44 transmitting the high magnitude forces associated with suction pump and levered
45 straining jaw movements (Dawson et al., 2011; Zweers, 1974; Zweers et al., 1977). In
46 duck, as in humans, the CP develops via a secondary cartilage intermediate (Solem et

47 al., 2011). Secondary cartilage requires proper mechanical stimulation for its induction
48 and maintenance, as confirmed by explant cultures and paralysis experiments, and is a
49 feature of many joints in neognathic avian skulls, as well as in select tendon and muscle
50 insertions (Hall, 1967, 1968, 1972, 1986). In paralyzed duck, secondary cartilage fails to
51 form at the CP, suggesting that the mechanical environment (i.e., function) during
52 development promotes secondary chondrogenesis (Solem et al., 2011). By comparison,
53 *Galliformes* like quail and chick, feed primarily by pecking seed, and this is reflected in
54 the relatively gracile construction of the jaw and adductor muscles, which insert dorsally
55 on the mandible and lack secondary cartilage on the CP. Exploiting such species-
56 specific differences in quail and duck, as we have done previously in studies of beak,
57 feather, cartilage, bone, and muscle patterning, (Ealba et al., 2015; Eames and
58 Schneider, 2008; Fish and Schneider, 2014a; Hall et al., 2014; Schneider, 2005, 2015;
59 Schneider and Helms, 2003; Tokita and Schneider, 2009) provides an opportunity to
60 investigate molecular, cellular, and biomechanical mechanisms that integrate form and
61 function in the jaw apparatus during development and evolution.

62
63 The species-specific jaw morphology that distinguishes duck from quail is mediated by
64 the neural crest mesenchyme (NCM), which gives rise to all of the associated cartilage,
65 bone, and muscle connective tissues (Noden and Schneider, 2006). Transplanting NCM
66 from quail into duck has established that NCM controls the size and shape of the jaw
67 skeleton, as well as the orientation and insertion of muscles (Ealba et al., 2015; Eames
68 and Schneider, 2008; Fish and Schneider, 2014a; Hall et al., 2014; Schneider and
69 Helms, 2003; Solem et al., 2011; Tokita and Schneider, 2009). Chimeric “quack” develop

70 a quail-like jaw musculoskeleton including a dorsal MA insertion that lacks secondary
71 cartilage. The precise developmental mechanisms through which this happens have
72 remained an open question. Presumably, for such a transformation, quail NCM alters
73 the duck-host environment in a manner that changes not only the form of the jaw
74 apparatus but also the function, since the presence or absence of secondary cartilage
75 depends upon proper mechanical cues. In this context, the lateral versus dorsal
76 insertion of the MA muscle might produce distinct mechanical forces, but differences in
77 the quantity and/or quality of such forces in quail versus duck are completely unknown.
78 Furthermore, those signaling pathways that are mechanoresponsive and ultimately
79 govern species-specific adaptation to the mechanical environment remain unclear. The
80 current study set out to address these unresolved issues.

81
82 We hypothesized that the form of the duck MA complex creates a species-specific
83 mechanical environment, which activates molecular programs for secondary
84 chondrogenesis at the CP. To test our hypothesis, we employed a range of strategies.
85 We modulated the form of the duck MA complex by titrating the amount of donor versus
86 host NCM-derived tissues in chick-duck chimeras. We quantified embryonic jaw motility
87 in duck versus quail and performed finite element analysis (FEA) to model the
88 mechanical environment of the MA complex. We employed FEA in order to make
89 predictions about the extent to which mechanical forces might underlie the induction of
90 secondary cartilage and the differential regulation of mechanically responsive signaling
91 pathways. We disrupted the mechanical environment of the MA complex by paralyzing
92 duck embryos and then we assayed for changes in signaling pathways that might be

93 mechanically responsive at the CP. After identifying candidate pathways, we tested if
94 they were necessary and/or sufficient for the formation of secondary cartilage.

95

96 Our results reveal that the formation of secondary cartilage on the CP depends upon
97 the amount and spatial distribution of NCM-derived connective tissues. While we
98 observe few quantitative differences in the amount of motility between quail and duck,
99 our FEA suggests that quail and duck have qualitatively distinct mechanical forces at
100 the MA insertion. Additionally, we discover that both FGF and TGF β signaling are
101 responsive to mechanical forces within the duck MA complex, and are necessary for
102 secondary chondrogenesis at the CP. Additionally, we find that exogenous FGF and
103 TGF β ligands can rescue cartilage in paralyzed duck and also induce cartilage in the
104 quail MA insertion, where ordinarily there is none. Overall, this study provides
105 mechanistic insights on how species-specific morphology, mechanical forces, and
106 resultant changes in signaling activity become integrated and contribute to
107 musculoskeletal plasticity. While form initially dictates function, function can also act as
108 a potent modulator of musculoskeletal form during development and evolution.

109

110 **Methods**

111 **The use of avian embryos**

112 Fertilized eggs of Japanese quail (*Coturnix coturnix japonica*) and white Pekin duck
113 (*Anas platyrhynchos*) were purchased from AA Lab Eggs (Westminster, CA) and
114 incubated at 37.5°C in a humidified chamber (GQF Hova-Bator, Savannah, GA) until
115 embryos reached stages appropriate for manipulations, treatments, and analyses. For

116 all procedures, we adhered to accepted practices for the humane treatment of avian
117 embryos as described in S3.4.4 of the AVMA Guidelines for the Euthanasia of Animals:
118 2013 Edition (Leary et al., 2013). Embryos were stage-matched using an approach that
119 is based on external morphological characters and that is independent of body size and
120 incubation time (Hamilton, 1965; Ricklefs and Starck, 1998; Starck and Ricklefs,
121 1998). The Hamburger and Hamilton (HH) staging system, originally devised for chick,
122 is a well-established standard (Hamburger and Hamilton, 1951). Separate staging
123 systems do exist for duck (Koecke, 1958) and quail (Ainsworth et al., 2010; Nakane and
124 Tsudzuki, 1999; Padgett and Ivey, 1960; Zacchei, 1961) but these embryos can also
125 be staged via the HH scheme used for chicken (Ainsworth et al., 2010; Le Douarin et
126 al., 1996; Lwigale and Schneider, 2008; Mitgutsch et al., 2011; Schneider and Helms,
127 2003; Smith et al., 2015; Starck, 1989; Yamashita and Sohal, 1987; Young et al.,
128 2014). Criteria utilized to align quail and duck at a particular HH stage change over time
129 depending on which structures become prominent. For early embryonic stages, we
130 used the extent of neurulation, NCM migration, and somitogenesis as markers (Fish et
131 al., 2014; Lwigale and Schneider, 2008; Schneider and Helms, 2003); whereas later, we
132 relied on growth of the limbs, facial primordia, feather buds, and eyes since these
133 become more diagnostic (Eames and Schneider, 2005; Merrill et al., 2008).

134

135 **Histology**

136 Embryos were fixed overnight in 10% neutral buffered formalin at 4°C, paraffin
137 embedded, and sectioned at 10µm. Cartilage, bone, muscle, and tendon were

138 visualized using Milligan's Trichrome or Safranin-O (Ferguson et al., 1998; Presnell and
139 Schreiber, 1997).

140

141 **Clearing and staining**

142 Embryos were fixed overnight at 4°C in 10% neutral buffered formalin before clearing
143 and staining with Alcian Blue and Alizarin Red to visualize cartilage and bone of the jaw
144 complex including the CP (Wassersug, 1976).

145

146 **cDNA preparation**

147 RNA was isolated from microdissected duck samples using the ARCTURUS PicoPure
148 RNA Isolation Kit (ThermoFisher, Waltham, MA). Reaction specifications and reverse
149 transcription programs were followed as previously published (Ealba and Schneider,
150 2013).

151

152 **In situ hybridization**

153 Spatial and temporal patterns of gene expression were analyzed by in situ hybridization
154 as previously described (Albrecht et al., 1997; Schneider et al., 2001). Species-specific
155 probes against duck FGF and TGF β ligands (*Fgf4*, *Fgf8*, *Tgf β 2*, *Tgf β 3*), receptors
156 (*Fgfr2*, *Fgfr3*, *Tgf β r2*), and downstream effectors (*Pea3*, *Erm*, and *Smad3*), were cloned
157 from duck HH33 cDNA libraries isolated from whole heads (Table S1). Probes were
158 designed to recognize all isoforms. High fidelity Pfu DNA polymerase (Stratagene, La
159 Jolla, CA) was used to amplify target genes. The protocol was: step 1, 2 minutes at
160 94°C; step 2, 30 seconds at 94°C; step 3, 30 seconds at 37.5°C; step 4, 2 minutes at

161 72°C; step 5, repeat steps 2 to 4 39 times; step 6, 5 minutes at 72°C; step 7, hold at
162 4°C. PCR products were run on a 1% agarose gel. Bands of the appropriate molecular
163 weight were gel extracted using QIAEX II Gel Extraction Kit (Qiagen, Hilden, Germany).
164 PCR products were ligated into pGEM-T Easy Vector System I (Promega, Madison, WI)
165 or CloneJET PCR Cloning Kit (ThermoFisher, Waltham, MA) and used to transform
166 NEB 5 α E. coli cells (New England Biolabs, Ipswich, MA). Clones were sequenced
167 (McLab, South San Francisco, CA) using a T7 promoter primer. Sequencing results
168 were analyzed using Geneious (Biomatters, Auckland, New Zealand). Once probe
169 sequences were confirmed, DIG-labeled RNA probes were synthesized using DIG RNA
170 labeling mix (Roche, Basel, Switzerland). Cloned species-specific duck probes were
171 used to identify gene expression patterns in embedded and sectioned HH33 and HH36
172 paralyzed and stage matched control duck.

173

174 **TUNEL staining**

175 10 μ m tissue sections of duck embryos 24 hours after treatment with SU5402,
176 SB431542, or DMSO soaked beads were processed using a fluorescent TUNEL
177 staining kit (Roche, Basel, Switzerland). As a positive control, DNase was added to a
178 subset of DMSO-treated tissue sections. The percentage of cell death was quantified
179 using 3D microscopy processing software Imaris (Bitplane, Belfast, United Kingdom).
180 Image intensity was rendered in 3D and Hoescht (Sigma-Aldrich, St. Louis, MO) and
181 TUNEL-stained nuclei within 100 μ m of the implanted bead were counted using
182 software-enabled volumetric criteria (surface detail=5 μ m, background

183 subtraction=12 μ m, seed point diameter=30 μ m). Statistical significance was determined
184 by ordinary one-way ANOVA (Prism 7, GraphPad Software, Inc., La Jolla, CA).

185

186 **Surgical bead implantation**

187 10mM of SU5402 (Sigma-Aldrich, St. Louis, MO), a small molecule that prevents
188 autophosphorylation of receptor tyrosine kinases and is most specific to FGFRs (Sun et
189 al., 1999; Sun et al., 1998), and 100mM of SB431542 (Santa Cruz Biotechnology, Santa
190 Cruz, CA), a small molecule that inhibits autophosphorylation of TGF β Rs (Callahan et
191 al., 2002; Inman et al., 2002), were diluted in DMSO. Formate bound AG1-X2 (50-100
192 mesh, 250-850 μ m, Bio-Rad, Hercules, CA) beads of about 250-350 μ m were washed in
193 DMSO at room temperature for about ten minutes before binding small molecule
194 inhibitors. 1mg/ml recombinant human FGF4 (R&D Systems, Minneapolis, MN) was re-
195 suspended in 0.1% filter sterilized BSA in 1x PBS. Heparin acrylic beads about 250-350
196 μ m (Sigma-Aldrich, St. Louis, MO) were used to deliver FGF4 to duck embryos. A
197 160 μ g/ml solution containing equal parts recombinant human TGF β 2 and TGF β 3 (R&D
198 Systems, Minneapolis, MN) was prepared using filter sterilized 4mM HCl in PBS
199 containing 0.1% BSA. Affigel Blue beads about 250-300 μ m (50-100 mesh, 150-300 μ m,
200 BioRad, Hercules, CA) were used to deliver TGF β ligands to quail and duck embryos.
201 Both FGF4 bound heparin acrylic beads and TGF β 2 and TGF β 3 bound Affigel Blue
202 beads were implanted into duck embryos to deliver a combination of all three ligands.
203 Beads were soaked in small molecule inhibitors or ligands for one hour at room
204 temperature before implantation. All concentrations were based on those used
205 previously (Eames and Schneider, 2008; Hayamizu et al., 1991; Niswander et al., 1993;

206 Schneider et al., 2001). Stage HH32 and HH33 embryos were housed in room
207 temperature incubators for one hour before surgeries to minimize embryonic motility.
208 For each bead type used, control surgeries were conducted using beads to deliver
209 carrier. All surgically implanted embryos were collected at HH38. Cleared and stained
210 cases with extensive cartilage and/or bone defects were excluded from analysis under
211 the assumption that a malformation in the jaw skeleton would adversely affect the native
212 mechanical environment. Two-tailed Fisher's exact test was used to determine
213 statistical significance (Prism 7, GraphPad).

214

215 **Endoscopy and jaw motility quantification**

216 *In ovo* video footage of quail and duck from HH32 to HH38 was recorded while eggs
217 incubated at 37.5°C. Video recordings were captured using a 1088 HD High Definition
218 Camera (Stryker, Kalamazoo, MI) with a 4mm, 30° arthroscope (Stryker, Kalamazoo,
219 MI). A universal, dual-quartz, halogen, fiber-optic light source (CUDA Surgical,
220 Jacksonville, FL) was threaded onto the endoscope to provide illumination. The
221 arthroscope was inserted through a small opening in the incubation chamber until it was
222 submerged in albumin. Embryos were acclimated to the light source for 15 minutes prior
223 to recording. Three 10-minute videos were collected from each embryo. The interval of
224 time from the first jaw movement to 5 seconds after the last jaw movement was defined
225 as an activity period, similar to a published quantification method (Hamburger et al.,
226 1965). Average percent active time was calculated along with 95% confidence intervals.
227 Significance was determined using an unpaired, two-tailed Holm-Sidak test adjusted for
228 multiple comparisons (Prism 7, GraphPad).

229

230 **3D reconstruction and finite element analysis**

231 To characterize species-specific differences in the biomechanical environment of the
232 jaw adductor complex, linear finite element analysis (FEA) was used to predict the
233 magnitude and distribution of the von Mises stress on the CP at the adductor insertion.
234 HH33 mandibles from duck and quail were serially sectioned (10 μ m thickness), stained
235 with Milligan's trichrome, and imaged at 2.5X magnification. Images were aligned using
236 the orbit and Meckel's cartilage as landmarks. Meckel's, the quadrate, surangular, and
237 the MA were manually segmented and reconstructed in 3D (Amira 6; FEI, Hillsboro,
238 OR). The resulting 3D reconstructions of the jaw complexes were imported into
239 commercial FEA software (ANSYS 17; Canonsburg, PA), which was used for meshing
240 and analysis. Tissues were meshed using tetrahedral elements, which were sized
241 based on convergence results from an iterative mesh refinement procedure. Final
242 models utilized 178,378 (duck) and 54,954 elements (quail). The material properties
243 calculated by Tanck et al. (2000) for mineralized embryonic mouse metatarsals
244 (Young's Modulus (E) = 117MPa; Poisson's Ratio (ν) = 0.3) were used for the
245 surangular and Meckel's. The other structures were suppressed prior to performing
246 FEA. Boundary conditions were prescribed to mimic those arising during jaw gaping,
247 and included: 1) a fixed support at the contact surface between Meckel's and the
248 quadrate; and 2) tensile force (duck 3.28E-04 N; quail 1.05E-04 N) aligned with the
249 longitudinal axis of the MA. The magnitudes of the adductor forces were determined
250 using cross-sectional area measurements performed at the longitudinal midpoints and
251 an assumed tensile stress of 1.11kPa (Landmesser and Morris, 1975). Statistical

252 significance was determined using an unpaired, two-tailed, t-test (Prism 7, GraphPad).

253

254 **Embryo paralysis**

255 HH32 or HH33 duck were paralyzed using 10mg/ml decamethonium bromide (DMBr)
256 (Sigma-Aldrich, St. Louis, MO) in Hank's Buffered Sterile Saline (HBSS) and filter
257 sterilized using a 0.22 μ m filter. Each embryo was treated with a 0.5ml dose of the DMBr
258 solution administered as previously described (Hall, 1986; Solem et al., 2011).

259

260 **Microdissections, RNA extraction, RT-qPCR, and analysis**

261 MA insertions were dissected from paralyzed and control duck embryos at HH33 and
262 HH36 and snap frozen in 70% EtOH mixed with dry ice. Microdissected samples were
263 homogenized using a bead-mill (Omni International, Kennesaw, Kentucky) and RNA
264 was isolated using the ARCTURUS PicoPure RNA Isolation Kit (ThermoFisher,
265 Waltham, MA). 200ng cDNA libraries were generated from RNA samples using iScript
266 reverse transcriptase (BioRad, Hercules, CA). Each cDNA library was subsequently
267 diluted to 2ng/ μ l. Duck *MYOD1*, *SOX9*, *TN-C*, and *UCHL-1* primer pairs were used to
268 determine the relative enrichment of muscle, cartilage, tendon, and nerve tissues,
269 respectively, relative to cDNA libraries from duck jaw complexes (Table S1). For quality
270 control, HH33 cDNA libraries were excluded from analysis if the sample was enriched
271 for muscle (>1-fold enrichment of *MYOD1* over control cDNA libraries), nerve (>1.5-fold
272 enrichment of *UCHL-1* over control cDNA libraries), or tendon (>2.5-fold enrichment of
273 *SOX9* over control cDNA libraries). At HH36, the top six tendon enriched samples with
274 less than 4-fold *MYOD1* enrichment were included in the analyses. *Fgf2*, *Fgf4*, *Fgf8*,

275 *Fgfr1, Fgfr2, Fgfr3, Pea3, Erm, Tgf β 2, Tgf β 3, Tgf β r1, Tgf β r2, Tgf β r3, Smad3, Smad7b,*
276 *and Pai1* expression was quantified by RT-qPCR using duck-specific primer pairs
277 (Table S1). For all genes, expression was normalized to *β -Actin* and analysis was done
278 following the $\Delta\Delta C(t)$ method (Ealba and Schneider, 2013; Livak and Schmittgen, 2001).
279 P-values for $-\Delta\Delta C(t)$ values were calculated using an unpaired, two-tailed, Holm-Sidak
280 test adjusted for multiple comparisons (Prism 7, GraphPad).

281

282 **Generation of chimeras**

283 GFP-chick (Crystal Bioscience, Emeryville, CA) and white Pekin duck eggs were
284 incubated to HH9. Tungsten needles and Spemann pipettes were used to graft two
285 differently sized populations of NCM from chick donors into stage-matched duck hosts,
286 producing chimeric “chuck” (Fish and Schneider, 2014a; Fish et al., 2014; Merrill et al.,
287 2008; Schneider, 1999; Schneider and Helms, 2003; Tucker and Lumsden, 2004).
288 Small grafts extended from the middle of the midbrain to the rostral hindbrain at
289 rhombomere 2, whereas large grafts extended from the forebrain–midbrain boundary to
290 rhombomere 2. Comparable-sized regions were excised from duck hosts. Orthotopic
291 grafts and sham operations were performed as controls. Controls and chimeras were
292 incubated side-by-side to ensure accurate staging during collections.

293

294 **Results**

295 **Adult jaw morphology is presaged during embryonic development**

296 There are many species-specific differences between Japanese quail and white Pekin
297 duck mandibles. Quail mandibles are slender with a smooth CP and diminutive

298 retroarticular process (Fig.1A). Duck mandibles feature a robust, laterally protruding CP.
299 Furthermore, duck mandibles are larger than quail, both absolutely and in relative
300 proportion, and have a sizeable retroarticular process (Fig.1B). Clearing and staining
301 reveals that species-specific jaw morphology is established during embryonic
302 development (Fig.1C,D). At HH38, an elongate Meckel's cartilage is surrounded by
303 lower jawbones, and the retroarticular processes are largely comprised of cartilage, yet
304 quail and duck morphologies are already distinguishable. The most obvious difference
305 is a secondary cartilage intermediate within the MA insertion along the surangular in
306 duck. Such cartilage is visible in cleared and stained duck as early as HH36. A
307 secondary cartilage never forms on quail or chick CP.

308

309 **NCM patterns the MA complex in a dose-dependent manner**

310 NCM transplanted from HH9 GFP-positive chick into stage-matched duck hosts
311 transforms the morphology of the jaw and CP (Fig.1E,F,I,J). The extent of
312 transformation and distribution of GFP-positive NCM-derived connective tissues
313 depends upon donor graft size. Small NCM transplants result in a limited distribution of
314 GFP-positive skeletal and connective tissues, and produce minor changes to the size
315 and shape of the jaw skeleton, but not enough to affect the secondary chondrogenesis
316 (Fig.1G,H). In contrast, large transplants result in extensively distributed GFP-positive
317 skeletal and connective tissues, and transform the jaw to become more chick-like,
318 including the absence of a secondary cartilage on the donor side CP (Fig.1K,L).

319

320 **The progression of embryonic jaw motility is similar in quail and duck**

321 *In ovo* videos of embryonic jaw motility captured periodic jaw gaping in quail and duck
322 embryos (Fig.2A,B,C,D)(Movie S1,S2). The first quantifiable jaw movements occur at
323 HH33 in quail and duck. HH33 quail are active 10.46% of the time (95% CI \pm 3.07%,
324 n=9) while stage-matched duck are active 5.2% of the time (95% CI \pm 1.06%, n=10).
325 Both the frequency and duration of jaw movements increase with developmental time in
326 quail and duck (Fig.2E,F). Quail and duck jaw motility track closely at HH34
327 (18.82% \pm 8.32%, n=12 for quail and 15.72% \pm 3.28%, n=18 for duck) and HH35
328 (28.58% \pm 16.63%, n=6 for quail and 29.35% \pm 6.57%, n=2 for duck). No statistically
329 significant differences in motility are observed in developmental stages preceding the
330 appearance of secondary cartilage. A significant difference is observed at HH36
331 (26.66% \pm 8.36%, n=22 for quail, and 43.97% \pm 5.06, n=26 for duck, p <0.0005), however,
332 by this stage, a secondary cartilage is already formed on the CP. Peak quail jaw motility
333 is observed at HH37 (67.39% \pm 5.7%, n=6 in quail, versus 51.72% \pm 8.69%, n=13 in duck)
334 while duck motility peaks at HH38, but does not exceed quail motility (60.76% \pm 5.79%,
335 n=7 in duck versus 61.67% \pm 5.49%, n=7 in quail).

336

337 **FEA predicts distinct mechanical environments at the quail and duck coronoid** 338 **process**

339 3D reconstructions of HH33 quail and duck jaws including Meckel's, the quadrate,
340 postorbital, surangular, and MA were created by manually segmenting histological
341 images (Fig.3A,B). Reconstructions reveal species-specific, geometrical differences in
342 cross-sectional area of the muscle, direction of contractile force, and area of the
343 surangular over which force is applied. In duck, the MA inserts on the lateral aspect of

344 the surangular, while in quail, the insertion is dorsal. In duck, the insertion is also more
345 proximal to the jaw joint. At its widest, the cross-sectional area of the duck MA is
346 $321,000\mu\text{m}^2$, while the slender quail muscle is only $114,192\mu\text{m}^2$ indicating the maximum
347 contractile force of the duck muscle is roughly 2.8 times greater than in quail.

348
349 Finite element models of the insertion site between the MA and the surangular predict
350 that duck experience a maximum shear stress concentration roughly 60 times greater
351 than quail (0.96MPa in duck versus 0.016MPa in quail)(Fig.3C,D). Furthermore, the
352 mean von Mises stress experienced in duck (0.053MPa) is significantly higher than in
353 quail (0.0045MPa; $p<0.0001$). Histograms also reveal the state of shear stress at the
354 insertion is more homogeneous in quail, while tissue at the duck insertion is subjected
355 to a broader range of shear stress (Fig.3E).

356

357 **The FGF pathway changes during development and is affected by paralysis**

358 RT-qPCR analyses on microdissected duck MA insertions reveal significant increases in
359 ligands *Fgf2* (5.34 ± 1.50 -fold change, $p<0.0005$), *Fgf4* (449.89 ± 237.59 -fold change,
360 $p<0.0005$), and *Fgf8* (56.22 ± 44.55 -fold change, $p<0.0005$) from HH33 to HH36 ($n=13$
361 for HH33 controls, $n=10$ for HH36 controls)(Fig.4A). FGF receptors *Fgfr1* (0.76 ± 0.21 -
362 fold change, $p<0.05$), *Fgfr2* (0.19 ± 0.18 -fold change, $p<0.0005$), and *Fgfr3* (0.68 ± 0.30 -
363 fold change, $p<0.05$) significantly diminish in expression over this time. Transcriptional
364 effectors *Pea3* (5.61 ± 1.09 -fold change, $p<0.0005$) and *Erm* (2.44 ± 0.54 -fold change,
365 $p<0.0005$) are both significantly more abundant at HH36 than at HH33.

366

367 Paralysis at HH32 does not result in significant changes to FGF signaling pathway
368 members or effectors at HH33 relative to stage-matched controls. In HH36 paralyzed
369 embryos, the only FGF ligand with a significant increase is *Fgf2* relative to HH33
370 controls (3.67 ± 1.30 -fold change, $p < 0.0005$) ($n=12$ for HH33 paralyzed, $n=11$ for HH36
371 paralyzed). However, *Fgf2* at HH36 is still significantly less in paralyzed embryos than in
372 stage-matched controls ($p < 0.05$) (asterisk, Fig.4A). In paralyzed HH36 embryos, *Fgf4* is
373 21.49 ± 33.68 -fold more abundant than in HH33 controls and *Fgf8* is 4.79 ± 5.06 -fold more
374 abundant, but both genes are still significantly less expressed than in stage-matched
375 controls ($p < 0.005$ for both) (asterisks, Fig.4A). At HH36, *Fgfr1* (0.55 ± 0.22 -fold change,
376 $p < 0.0005$) and *Fgfr2* (0.35 ± 0.29 -fold change, $p < 0.0005$) are significantly down in
377 paralyzed samples, similar to expression dynamics seen in controls over the same
378 period. Unlike control samples, *Pea3* (2.58 ± 2.75 -fold change) and *Erm* (1.49 ± 0.67 -fold
379 change) remain relatively flat in paralyzed embryos and, by HH36, are significantly less
380 abundant than in HH36 controls ($p < 0.05$ for both) (asterisks, Fig.4A).

381
382 Analysis of spatial and temporal gene expression patterns was conducted in control and
383 paralyzed duck at HH33 and HH36 (Table 1). At HH33, in sagittal section, the MA is
384 visible as two muscle bundles divided proximodistally by the mandibular branch of the
385 trigeminal nerve (Fig.4B). Proximal to the mandibular nerve, the MA appears fan-like
386 and inserts broadly. Distal to the nerve, unipinnate muscle fibers are joined by a fibrous
387 aponeurosis. The musculature and aponeurosis appear relatively disorganized following
388 24 hours of paralysis (Fig.4F).

389

390 At HH33, *Fgf4* is expressed throughout primary cartilages like the quadrate, and
391 Meckel's, as well as in skeletal muscles like the MA, the MA insertion, and the
392 mesenchymal condensation that will give rise to secondary cartilage (n=5 for each
393 gene)(Fig.4C). After 24 hours of paralysis, *Fgf4* is maintained in the quadrate and
394 Meckel's, but diminished in the MA and its insertion (Fig.4G). *Fgf8* is in the MA, the MA
395 insertion, the secondary cartilage insertion, and the surangular condensation (Fig.S1).
396 There is also *Fgf8* in primary cartilages like Meckel's and the quadrate. The secondary
397 cartilage condensation and its *Fgf8* domain are not present in embryos 24 hours after
398 paralysis (Fig.S1). *Fgfr2* is in the quadrate and Meckel's, particularly in the
399 perichondrium, as well as in the secondary cartilage condensation and the nascent
400 surangular (Fig.4D). Following 24 hours of paralysis, expression in primary cartilage is
401 maintained, while expression in the secondary cartilage condensation and surangular
402 condensation are diminished (Fig.4H). *Fgfr3* is in the quadrate and Meckel's, but not
403 perichondria, and in the surangular condensation with greater expression around the
404 periphery (Fig.4E). Paralysis leads to decreased expression in the surangular
405 condensation while expression in primary cartilage is maintained (Fig.4I). *Pea3* is in the
406 MA, the MA insertion and the secondary cartilage condensation (Fig.S1). There is also
407 expression in the surangular condensation, primary cartilages and perichondria. 24
408 hours after paralysis, the secondary cartilage condensation fails to form and the
409 corresponding region of *Pea3* is absent (Fig.S1).

410

411 By HH36, secondary cartilage is present within the MA insertion and is encapsulated in
412 a dense fibrous sheath (Fig.4J). The MA muscles have begun to separate into distinct

413 superficial sheet-like, proximal fan-like, and distal groups of fibers. HH36 paralyzed
414 embryos have poor muscle and tendon organization and lack a secondary cartilage
415 condensation (Fig.4N). *Fgf4* (n=5 for each gene) is strongly expressed at HH36 in the
416 MA, the MA insertion, and the surangular and periosteal (Fig.4K). The quadrate and
417 Meckel's also express *Fgf4* throughout the cartilage and perichondrium. *Fgf4* is also
418 seen within the secondary cartilage condensation. Paralysis prevents secondary
419 chondrogenesis, however, *Fgf4* is maintained in muscle, bone, and primary cartilages
420 (Fig.4O). *Fgf8* is in the MA, tendon, and secondary cartilage (Fig.S1). *Fgf8* is also in
421 the surangular, periosteum, and primary cartilage. Paralysis prevents secondary
422 cartilage from forming, but *Fgf8* is still in muscle and its connective tissues (Fig.S1).
423 *Fgfr2* is in muscle, tendon, bone, periosteal, cartilage, perichondria, and within
424 secondary cartilage (Fig.4L). Following paralysis, the only change to *Fgfr2* is the
425 absence of a secondary cartilage domain (Fig.4P). *Fgfr3* is in the quadrate and
426 Meckel's as well as in the periosteum of the surangular. *Fgfr3* is also in muscle, tendon,
427 bone, periosteal, cartilage, perichondria, and secondary cartilage (Fig.4M). Expression
428 in the secondary cartilage is highest at the center and grows lower towards the
429 periphery. In paralyzed embryos, only the *Fgfr3* domain in secondary cartilage is absent
430 (Fig.4Q). *Pea3* is in the MA muscle, tendon, and the secondary cartilage condensation
431 (Fig.S1). *Pea3* is also in primary cartilage, perichondria, bone, and periosteal. As
432 secondary cartilage fails to form in HH36 paralyzed embryos, *Pea3* is absent (Fig.S1).

433

434 **The TGF β pathway changes during development and is affected by paralysis**

435 Quantitative RT-PCR shows that *Tgfβ2* (4.28±1.29-fold change, p<0.0005) and *Tgfβ3*
436 (7.19±2.11-fold change, p<0.0005) increase significantly from HH33 to HH36 (n=10 for
437 HH33 controls, n=10 for HH36 controls)(Fig.5A). Paralyzed embryos mirror the
438 increases in *Tgfβ2* (2.87±1.36-fold change, p<0.05) and *Tgfβ3* (5.50±2.30-fold change,
439 p<0.0005) over the same period. Transcriptional activity of receptors *Tgfβr1*, *Tgfβr2*,
440 *Tgfβr3*, and transcriptional effectors *Smad3*, *Smad7b*, and *Pai1* remain flat in controls.
441 In contrast, HH36 paralyzed samples express more *Pai1* (2.53±1.89-fold change) than
442 HH33 controls (p<0.05), and achieve significantly greater expression than HH36 control
443 samples (p<0.05)(asterisk, Fig.5A).

444

445 Our qualitative analyses show that at HH33, *Tgfβ2* is expressed in the MA muscle, the
446 MA insertion, and the secondary cartilage condensation (Fig.5B,C). At HH33, following
447 24 hours of paralysis, expression in muscle and tendon persists while the secondary
448 cartilage condensation and its *Tgfβ2* domain does not (Fig.5F,G). *Tgfβ3* is also in the
449 MA muscle, the MA insertion, primary cartilage like Meckel's and the quadrate, and the
450 secondary cartilage condensation (Fig.5D). At this stage, the only *Tgfβ3* domain
451 affected by paralysis is in the secondary cartilage condensation (Fig.5H). *Tgfβr2* is in
452 the MA, the MA insertion, and in the secondary cartilage condensation (Fig.5E). *Tgfβr2*
453 is also in Meckel's and the quadrate. Following paralysis, the only expression domain
454 affected is the secondary cartilage condensation (Fig.5I). *Smad3* is in the MA, the
455 insertion, and the secondary cartilage condensation (Fig.S1). *Smad3* is also in the
456 quadrate, Meckel's, and other primary cartilages. The secondary cartilage domain does
457 not appear in stage-matched, paralyzed embryos (Fig.S1).

458

459 In HH36 duck, *Tgfβ2* is in muscles like the MA, tendons like the MA insertion, bones like
460 the surangular and their periosteal, and cartilages like Meckel's, the quadrate, and their
461 perichondria (Fig.5K). *Tgfβ2* is also expressed throughout the secondary cartilage on
462 the CP. Following paralysis, the only change in expression at HH36 is for *Tgfβ2*
463 coincident with the loss of secondary cartilage (Fig.5O). *Tgfβ3* is in all the same tissues
464 as *Tgfβ2* in HH36 control and paralyzed embryos, including the secondary cartilage
465 (Fig.5L,P). By HH36, *Tgfβr2* is in the surangular, as well as secondary cartilage on the
466 CP (Fig.5M). Following paralysis, the secondary cartilage and its *Tgfβr2* domain are
467 absent while *Tgfβr2* in bone is unaffected (Fig.5Q). *Smad3* is in the MA and its insertion,
468 and in the secondary cartilage. There is also *Smad3* in primary cartilages, perichondria,
469 bone, and periosteal (Fig.S1). Paralyzed HH36 embryos do not form secondary cartilage
470 so the corresponding *Smad3* expression is absent (Fig.S1).

471

472 **Inhibiting FGF or TGFβ signaling affects the condensation of secondary cartilage**

473 Unilateral delivery of FGF signaling inhibitor SU5402 blocks the formation of, or reduces
474 the size of secondary cartilage on the CP (n=18 at HH32, n=29 at HH33)(Fig.6A,C). No
475 change in secondary cartilage is observed following delivery of DMSO control beads
476 (n=6). The efficacy of secondary cartilage inhibition at HH38 depends upon the stage of
477 treatment, with HH32 embryos being more sensitive to FGF inhibition than HH33
478 embryos (Fisher's exact test, p=0.0047). In 88.9% of embryos treated with SU5402 at
479 HH32, secondary cartilage is either lost or reduced in size (n=16/18). Of those
480 secondary cartilage phenotypes, 50% are reduced in size (n=8/16), and 50% have a

481 complete absence (n=8/16) of secondary cartilage. FGF inhibition at HH33 reduces the
482 size of the secondary cartilage in 31.01% of cases (n=9/29) and prevents secondary
483 cartilage induction in 13.79% of cases (n=4/29).

484

485 Inhibition of TGF β signaling by delivering SB431542 also frequently causes loss or
486 reduction in the size of the secondary cartilage on the CP (n=37 at HH32, n=66 at
487 HH33)(Fig.6 B,D). Although the statistical distribution of outcomes does not depend on
488 whether embryos are treated at HH32 (40.54% absent or reduced secondary cartilage,
489 n=15/37) or HH33 (39.39% absent or reduced secondary cartilage, n=26/66), HH32
490 treatments tend to be more efficacious at preventing secondary chondrogenesis
491 (13.51%, n=5/37) than HH33 treatments (3.03%, n=2/66).

492

493 **Inhibiting FGF or TGF β signaling does not lead to increased cell death**

494 TUNEL staining shows that implanting AG1X2 chromatography beads soaked in DMSO
495 (n=3 embryos) or small molecule inhibitors of FGF signaling (n=6 embryos) or TGF β
496 signaling (n=7 embryos) at HH32 does not increase cell death nor did we observe
497 histological evidence at any stage where muscle or tendon formation were blocked by
498 treatment delivery (data not shown). 24 hours after implantation, 0.69% of cells
499 surrounding DMSO soaked beads are undergoing apoptosis (n=5 sections)(Fig.6E,F).
500 There is no significant increase in cell death over control beads with SU5402 (1.42%,
501 n=19 sections) or SB431542 (0.22%, n=29 sections)(Fig.6H,I) treatments. For
502 comparison, DNase-treated positive control slides show significantly more cell death
503 (52.60%, n=3 sections, unpaired t-test p<0.0001)(Fig.6G).

504

505 **Exogenous FGF and TGF β treatments can restore cartilage in paralyzed embryos**

506 HH38 duck embryos paralyzed and treated with FGF4 beads at HH32 form cartilage
507 adjacent to or surrounding the bead in 27.27% of cases (n=3/11)(Fig.7B). No cartilage is
508 induced in any embryos treated with BSA beads alone (n=4 heparin acrylic, n=12 Affigel
509 blue)(asterisk, Fig.7A), or in cases where recombinant protein soaked beads are
510 located far from the MA insertion (n=4 for FGF4, n=2 for TGF β 2/TGF β 3, and n=4 for
511 FGF4/TGF β 2/TGF β 3). Paralysis and implantation of beads soaked in TGF β 2 and
512 TGF β 3 induce cartilage in 75% of HH38 duck (n=15/20)(Fig.7C). Implanting both FGF4
513 and TGF β 2/TGF β 3 soaked beads in paralyzed HH32 duck induces cartilage in 85.71%
514 of cases (n=12/14)(Fig.7D). Treating HH32 quail with exogenous TGF β 2/TGF β 3
515 induces a chondrogenic response in 11.11% of embryos (n=1/9)(Fig.7E). Safranin-O
516 staining confirms the presence of a glycosaminoglycan-rich cartilaginous extracellular-
517 matrix surrounding the beads (n=2/3)(Fig.7F). Although spherical beads were
518 implanted, the axial orientation of Safranin-O-positive tissue surrounding the beads is
519 not radially symmetrical and tends to align with the orientation of the MA insertion.
520 Analysis of paralyzed duck rescue experiments reveal that the distribution of
521 phenotypes depends upon the ligand or ligands received (Fisher's Exact Test,
522 p=0.005)(Fig.7G).

523

524 **Discussion**

525 **NCM controls the species-specific pattern of the MA insertion**

526 In previous studies we have shown that NCM controls the species-specific size and
527 shape of the jaw skeleton and associated musculature via cell-autonomous
528 morphogenetic programs (Solem et al., 2011; Tokita and Schneider, 2009). But in the
529 present study we go further and substantiate that this patterning ability is dose-
530 dependent. While we know that the extent of gene expression in chimeras is directly
531 related to the degree of chimerism (Ealba and Schneider, 2013), here we were able to
532 extend this principle to morphology and modulate the presence or absence of
533 secondary cartilage on the CP by titrating the size of donor NCM transplants and thus
534 the distribution of NCM-derived connective tissues. Small transplants did not alter
535 secondary cartilage development whereas larger transplants did. Based on our prior
536 analyses of muscle and connective tissue patterning (Solem et al., 2011; Tokita and
537 Schneider, 2009), and the critical role for interactions between NCM and muscle
538 precursors (Bothe et al., 2007; Evans and Noden, 2006; Grenier et al., 2009; Noden,
539 1983, 1988; Noden and Trainor, 2005; Rinon et al., 2007), we expect that increasingly
540 larger populations of donor NCM relocate the MA insertion from a duck-like lateral
541 position to one that is more dorsal and chick-like. In this way, and concomitant with its
542 patterning abilities, NCM would be acting as a major determinant of the mechanical
543 environment whereby specific loading conditions are more conducive to secondary
544 cartilage formation.

545

546 **Quality not quantity of mechanical stimulation drives secondary chondrogenesis**

547 Secondary cartilage development can be divided into two phases: induction and
548 maintenance. Both phases require proper biomechanical stimulation. Embryonic motility

549 is an essential source of biomechanical stimulation and the developmentally plastic
550 response to biomechanical loading is a potent mechanism through which embryonic
551 form comes to presage adult function (Anthwal et al., 2015; Blitz et al., 2009; Brunt et
552 al., 2017; Carter and Beaupré, 2007; Hall, 1967, 1968, 1972, 1986; Hall and Herring,
553 1990; Havis et al., 2016; Huang et al., 2013; Kardon, 1998; Pitsillides, 2006; Pollard et
554 al., 2014; Schweitzer et al., 2010; Sharir et al., 2011; Shwartz et al., 2012; Solem et al.,
555 2011; Wu et al., 2001). For induction of secondary cartilage to occur, the frequency of
556 mechanical stimulation must cross a threshold (Hall, 1967, 1968). The size of a
557 secondary cartilage can also be decreased by paralysis after secondary cartilage
558 induction (Solem et al., 2011). The similarity in early quail and duck jaw motility
559 indicates that frequency of jaw activity is an unlikely determinant of species-specific
560 secondary chondrogenesis. A significant difference in motility manifests at HH36,
561 though a secondary cartilage is already formed in duck by that time. Thus, we conclude
562 that the frequency of mechanical stimulation is not, itself, sufficient to induce secondary
563 cartilage in quail versus duck, which points to the role of biomechanical stress resulting
564 from a combination of species-specific muscle pattern and resultant differences in the
565 quality or type of functional loading on the muscle insertion.

566

567 **Mechanical cues result from and contribute to species-specific morphology**

568 Prior work has highlighted the contribution of the mechanical environment in wrap-
569 around and other force-transmitting tendons (Benjamin and Ralphs, 1998; Blitz et al.,
570 2013; Carter and Beaupré, 2007; Murchison et al., 2007; Schweitzer et al., 2010;
571 Shwartz et al., 2013). Such a configuration, in which a tendon experiences not only axial

572 tension, but also compression in which the tendon is held taught against the bone, is
573 conducive to fibrocartilage development (Blitz et al., 2009; Koo et al., 2017). Thus, the
574 evolutionary presence or absence of secondary cartilage on the CP reflects species-
575 specific variation in functional anatomy determined by *in ovo* mechanical loading
576 (Beresford, 1981; Fang and Hall, 1997; Hall, 1979; Stutzmann and Petrovic, 1975). In
577 taxa such as humans, rats, cats, and duck, secondary cartilage forms at the jaw
578 adductor muscle insertion (Amorim et al., 2010; Amorim et al., 2008; Hall, 2005;
579 Horowitz and Shapiro, 1951; Kantomaa and Rönning, 1997; Moore, 1973, 1981; Solem
580 et al., 2011; Soni and Malloy, 1974; Vinkka, 1982; Washburn, 1947) whereas an
581 equivalent secondary cartilage is absent in mice, guinea pigs, chick, and quail (Anthwal
582 et al., 2008; Anthwal et al., 2015; Boyd et al., 1967; Moss and Meehan, 1970; Rot-
583 Nikcevic et al., 2007; Shibata et al., 2003; Solem et al., 2011). Our work implies that the
584 reason secondary cartilage forms at this location in some species and not others is due
585 to the way NCM-mediated muscle pattern leads to differential forces during embryonic
586 motility.

587
588 To our knowledge, this is the first finite element modelling of the embryonic jaw
589 adductor complex. Our FEA illuminates the difference in both the predicted magnitude
590 and spatial distribution of von Mises stress in the MA insertion of embryonic quail and
591 duck prior to secondary chondrogenesis. Perhaps the wide ranging magnitudes of shear
592 stress distributed across the surface of the duck surangular mediates the precise
593 biomechanical cues required to elicit a spatially restricted domain of secondary
594 cartilage. The secondary cartilage is the future site of an ossification center that fuses to

595 the surangular, enables robust osteointegration, and further distinguishes both the form
596 and the functional mechanics of the duck versus quail jaw apparatus. However, the
597 mechanisms that facilitate the relationship between mechanical stimulation and
598 musculoskeletal adaptation have remained largely unknown. While previous studies
599 have implicated FGF and TGF β signaling in both early, muscle-independent, and late,
600 muscle-dependent, phases of sclerotome-derived limb tendons (Havis et al., 2016;
601 Havis et al., 2014; Huang et al., 2015), our findings suggest that mechanical cues drive
602 differential activation of FGF and TGF β signaling to induce species-specific secondary
603 cartilage within an NCM-derived tendon insertion. Moreover, we do not observe any
604 evidence for crosstalk between these pathways, given that paralysis downregulates
605 FGF signaling while TGF β expression remains unchanged. Conversely, despite the
606 maintenance of TGF β , FGF is downregulated. Such findings are consistent with the
607 independent functions of these pathways during chick limb tendon morphogenesis
608 (Havis et al., 2016). However, manipulating these pathways in the limb has not been
609 shown to induce cartilage formation.

610

611 **FGF and TGF β are necessary and sufficient for secondary chondrogenesis**

612 Molecular programs of tendon development are context-dependent. In mouse limbs,
613 TGF β signaling promotes tendon development while FGF signaling is inhibitory (Blitz et
614 al., 2013; Havis et al., 2014; Pryce et al., 2009; Subramanian and Schilling, 2015).
615 However, FGF signaling is a pro-tendon signal in chick limbs and promotes axial mouse
616 and chick tendon development (Brent et al., 2005; Brent et al., 2003; Edom-Vovard et
617 al., 2001; Edom-Vovard et al., 2002; Havis et al., 2016; Havis et al., 2014; Smith et al.,

618 2005). Our quantitative and qualitative analyses demonstrate that FGF and TGF β
619 ligands, receptors, and effectors are expressed in musculoskeletal tissues throughout
620 stages important for secondary cartilage induction and maintenance, and paralysis has
621 a significant but differential effect on transcription of some of these genes. We find that
622 *Fgf4* and *Fgf8* are dramatically affected by paralysis, indicating that their expression
623 may be mediated by mechanical stimulation. Furthermore, FGF signaling activity is
624 decreased following paralysis as indicated by the relative down regulation of *Pea3* and
625 *Erm* transcription. While the role of FGF signaling in the context of cartilage, bone,
626 muscle, and limb tendon is well described (Brent et al., 2005; Edom-Vovard et al., 2001;
627 Eloy-Trinquet et al., 2009; Murakami et al., 2000; Ornitz and Marie, 2015), the influence
628 of the mechanical environment on FGF signaling has remained unclear. While we do
629 not observe an effect of paralysis on the transcription of TGF β ligands or receptors, the
630 downstream effector *Pai1* was significantly increased by paralysis, suggesting tissue
631 atrophy and fibrosis in response to disuse (Naderi et al., 2009). There is a relationship
632 between the mechanical environment and TGF β signaling (Kleinnulend et al., 1995;
633 Nguyen et al., 2013; Robbins et al., 1997; Shi et al., 2011), but how mechanical cues
634 exert control over TGF β signaling is not as well understood. Our results suggest that, in
635 this context, TGF β signaling activity is primarily regulated by post-transcriptional
636 modifications like phosphorylation of SMADs (Anthwal et al., 2008; Berthet et al., 2013;
637 Maeda et al., 2011; Wipff et al., 2007) and regulation of free, active TGF β ligands,
638 something we plan to pursue in future studies.

639

640 Knockouts of *Tgfβ2* and *Tgfβr2* in mice produce malformations of the dentary and its
641 coronoid, condylar, and angular processes (Oka et al., 2008; Oka et al., 2007; Sanford
642 et al., 1997), although, the malformations of the three processes likely arise via different
643 mechanisms. Also, unlike duck and humans, the mouse coronoid process does not form
644 via a secondary cartilage intermediate. In *Tgfβ2* null mice, the condylar and angular
645 processes are smaller, but the secondary cartilages on these processes persist.
646 However, secondary chondrogenesis was prevented by *Tgfβr2* knockout. Mandible
647 culture experiments in mice also demonstrate that TGFβ signaling is required for
648 condylar and angular secondary cartilage induction (Anthwal et al., 2008). In the context
649 of our experiments, TGFβ inhibition does not produce bone defects, nor do we observe
650 abnormalities in Meckel's. This is consistent with TGFβ knockout data in which tendon
651 formation is severely inhibited in the absence of *Tgfβ2*, *Tgfβ3*, or *Tgfβr2*, while primary
652 cartilage is largely unperturbed (Pryce et al., 2009).

653
654 Our efforts to rescue paralyzed embryos led to the formation of a dense fibrous capsule
655 and even cartilage around the bead. Although ligands were delivered using spherical
656 beads and presumably diffused uniformly (Eichele et al., 1984), the axis of Alcian blue
657 or Safranin-O positive tissue surrounding the beads is not radially symmetrical.
658 Directional distribution of induced cartilage in quail and duck suggests that the
659 mesenchyme and surrounding connective tissues overlying the surangular are not all
660 equivalent in their capacity to generate secondary cartilage. Furthermore, the locations
661 where cartilage is induced are spatially restricted to the general region where secondary
662 cartilage forms in controls. Such a spatial constraint parallels published explant data in

663 which the murine CP, which does not ordinarily form a secondary cartilage, can be
664 induced to do so by fetal bovine serum (FBS)(Anthwal et al., 2015). Though FBS bathed
665 the entire mandible, ectopic cartilage was only observed on the CP. In duck and quail,
666 beads implanted too distal from the jaw joint, or too superficial, superior, or inferior to
667 the surangular did not elicit a chondrogenic response.

668

669 Other experiments on developing limb tendons corroborate the ability of exogenous
670 FGF and TGF β ligands to maintain *Scx* even in the absence of mechanical stimulation,
671 but to our knowledge, no instances of induced cartilage have been reported in those
672 contexts (Edom-Vovard et al., 2002; Havis et al., 2016). The FGF and TGF β signaling-
673 dependent chondrogenic response we observed may be localized to tendon and
674 connective tissues surrounding the MA insertion and is conserved between quail and
675 duck. Though quail do not normally form secondary cartilage on their CP, the
676 surrounding connective tissues are able to do so given the proper signaling
677 environment.

678

679 Induced cartilage appears to be encapsulated and distinct from the surangular,
680 mirroring native secondary cartilage development on the duck CP. Thus, the secondary
681 cartilage on the CP is likely derived from cells in the tendon and adjacent connective
682 tissue, not the periosteum as in articular secondary cartilage (Buxton et al., 2003).
683 Experiments in other contexts suggest the existence of progenitor cells that express
684 both tendon (e.g., *Scx*, *Tcf4*) and cartilage (e.g., *Sox9*) tissue markers that contribute
685 functionally to establishing certain sites where tendons or ligaments insert onto primary

686 cartilage and that such markers are involved in the patterning of these insertions (Blitz
687 et al., 2013; Kardon, 1998; Kardon et al., 2003; Mathew et al., 2011; Schweitzer et al.,
688 2001; Sugimoto et al., 2013). Cells that give rise to secondary cartilage on the CP may
689 express a similar complement of lineage markers, which is supported by our previous
690 expression analyses (Solem et al., 2011; Tokita and Schneider, 2009).

691

692 **Mechanical cues differentially regulate members of the FGF and TGF β pathways**

693 Clearly, musculoskeletal development and homeostasis depend upon proper
694 biomechanical cues, however, the cell-biology that mediates this mechanosensation is
695 not well understood. A variety of mechanisms including the primary cilium, Wnt
696 signaling, and especially sclerostin, which is an osteocyte-specific Wnt inhibitor, have
697 been implicated in mechanosensitive bone remodeling (Robling et al., 2016; Robling et
698 al., 2008; Rolfe et al., 2014; Tu et al., 2012). Other potential mechanisms may include
699 ligands being freed from the extracellular matrix, ion channels, focal adhesions,
700 cytoskeletal dynamics, and many others (del Rio et al., 2009; Dupont et al., 2011;
701 Hamill and McBride, 1996; Maeda et al., 2011; Mammoto and Ingber, 2010; Matthews
702 et al., 2006; McBeath et al., 2004; Pruitt et al., 2014; Quinn et al., 2002; Raizman et al.,
703 2010; Ramage et al., 2009; Roberts et al., 2001; Shakibaei and Mobasheri, 2003;
704 Solem et al., 2011; Vincent et al., 2002; Vincent et al., 2007; Wang et al., 2009; Wen et
705 al., 2017).

706

707 From our qualitative and quantitative analyses, a subset of genes stands out as likely
708 mediating development of the MA complex (*Tgfb2*, *Tgfb3*, *Fgfr1*, and *Fgfr2*) as their

709 abundance changes significantly and in the same direction regardless of whether the
710 embryo was paralyzed or not (Fig.8A). This group of genes includes *Tgfβ2* and *Tgfβ3*,
711 which induce chondrogenesis when delivered as ligands to paralyzed duck embryos or
712 normal developing quail, suggesting that TGFβ signaling activity may be modulated
713 post-transcriptionally and depend upon the availability of free, active TGFβ ligands.
714 Also, we observed no change in *Tgfβr1*, *Tgfβr2*, *Tgfβr3*, *Smad3*, or *Smad7b*. Our
715 analyses did find that one component of the TGFβ pathway is significantly more
716 abundant in paralyzed samples. *Pai1*, a common transcriptional readout of TGFβ
717 signaling (Kawarada et al., 2016), became significantly more abundant following
718 paralysis. Our data support the hypothesis that TGFβ pathway-mediated responses to
719 mechanical stimulation utilize post-transcriptional mechanisms. Quantifying free, active
720 TGFβ ligands, or assaying phospho-SMAD abundance or nuclear localization would
721 shed light on this phenomenon, something that we are working towards for future
722 studies.

723
724 Our analyses also indicate that a second set of five FGF signaling pathway components
725 (*Fgf2*, *Fgf4*, *Fgf8*, *Pea3*, and *Erm*) likely mediates normal development of secondary
726 cartilage and depends upon embryonic muscle contractions to maintain their activation.
727 FGF signaling has been implicated in other mechanosensitive processes (Vincent et al.,
728 2002; Vincent et al., 2007; Wen et al., 2017), but there is still a lot to learn about how
729 FGF ligands, receptors, and transcriptional effectors interact with the mechanical
730 environment.

731

732 Our data suggest a model (Fig.8) whereby species-specific secondary chondrogenesis
733 on the CP arises as a consequence of functional motility acting upon NCM-derived
734 form. In our model, the resulting stress within the insertion of the MA muscle onto the
735 surangular differentially activates FGF and TGF β signaling, which are each necessary
736 and sufficient to induce chondrogenesis. Thus, by balancing cell-autonomous
737 developmental programs and adapting to environmental cues, NCM generates species-
738 specific jaw geometry and promotes structural and functional integration of the
739 musculoskeletal system during development.

740
741 E.S. Russell in his classic book, *Form and Function* (1916) poses the question, “Is
742 function the mechanical result of form, or is form merely the manifestation of function or
743 activity? What is the essence of life, organisation or activity? (p.v)” Our findings provide
744 evidence that form initially dictates function but then function modulates form. Cranial
745 NCM establishes species-specific “organisation” prior to the onset of muscle “activity.”
746 However, the musculoskeleton is developmentally plastic. As jaw activity begins, form
747 adapts to meet and support functional demands. In the case of a duck, species-specific
748 form, coupled with jaw activity, creates stresses within the MA insertion, differentially
749 activates FGF and TGF β signaling, and induces secondary cartilage on the CP.
750 Appreciating the inextricable connection between form and function allows for a new
751 perspective on the role of NCM in establishing form but also shows how the organism
752 can modify that form to accommodate functional demands throughout development,
753 under selective pressure, or in disease states.

754

755 **Acknowledgements**

756 We thank J. Lotz, T. Alliston, R. Marcucio, J. Fish, and members of the Schneider lab
757 for helpful discussions; Z. Vavrusova, M. Bodendorfer (Hague), D. Jaul, M. Chung, S.
758 Smith, and D. Chu for technical assistance; and T. Dam at AA Lab Eggs for quail and
759 duck eggs. This work was supported in part by NICHD T32 HD007470 and F31
760 DE024405 to K.C.W.; and NIDCR R01 DE016402, R01 DE025668, and S10 OD021664
761 to R.A.S.

762

763 **Author Contributions**

764 R.A.S. and K.C.W. conceived of the project and designed the experiments; K.C.W.
765 S.G., and S.H. performed the experiments; K.C.W. S.G., S.H., A.F., and R.A.S.
766 analyzed the data; and R.A.S. and K.C.W. co-wrote the manuscript.

767

References

- 768
769
770 Albrecht, U., Eichele, G., Helms, J.A., Lu, H.-C., 1997. Visualization of gene expression
771 patterns by in situ hybridization. *Molecular and cellular methods in developmental*
772 *toxicology*, 23-48.
- 773 Amorim, M.M., Borini, C.B., de Castro Lopes, S.L., de Oliveira Tosello, D., Berzin, F.,
774 Caria, P.H., 2010. Relationship between the angle of the coronoid process of the
775 mandible and the electromyographic activity of the temporal muscle in skeletal Class I
776 and III individuals. *Journal of oral rehabilitation* 37, 596-603.
- 777 Amorim, M.M., Borini, C.B., Lopes, S.L., Haiter-Neto, F., Berzin, F., Caria, P.H., 2008.
778 Relationship between the inclination of the coronoid process of the mandible and the
779 electromyographic activity of the temporal muscle in skeletal Class I and II individuals.
780 *Journal of oral science* 50, 293-299.
- 781 Anthwal, N., Chai, Y., Tucker, A.S., 2008. The role of transforming growth factor-beta
782 signalling in the patterning of the proximal processes of the murine dentary. *Dev Dynam*
783 237, 1604-1613.
- 784 Anthwal, N., Peters, H., Tucker, A.S., 2015. Species-specific modifications of mandible
785 shape reveal independent mechanisms for growth and initiation of the coronoid.
786 *EvoDevo* 6.
- 787 Benjamin, M., Ralphs, J.R., 1998. Fibrocartilage in tendons and ligaments--an
788 adaptation to compressive load. *J Anat* 193 (Pt 4), 481-494.
- 789 Beresford, W.A., 1981. Chondroid bone, secondary cartilage, and metaplasia. Urban &
790 Schwarzenberg, Baltimore, Md.
- 791 Berthet, E., Chen, C., Butcher, K., Schneider, R.A., Alliston, T., Amirtharajah, M., 2013.
792 Smad3 binds Scleraxis and Mohawk and regulates tendon matrix organization. *J Orthop*
793 *Res* 31, 1475-1483.
- 794 Blitz, E., Sharir, A., Akiyama, H., Zelzer, E., 2013. Tendon-bone attachment unit is
795 formed modularly by a distinct pool of Scx- and Sox9-positive progenitors. *Development*
796 140, 2680-2690.
- 797 Blitz, E., Viukov, S., Sharir, A., Shwartz, Y., Galloway, J.L., Pryce, B.A., Johnson, R.L.,
798 Tabin, C.J., Schweitzer, R., Zelzer, E., 2009. Bone Ridge Patterning during
799 Musculoskeletal Assembly Is Mediated through SCX Regulation of Bmp4 at the
800 Tendon-Skeleton Junction. *Developmental Cell* 17, 861-873.
- 801 Bothe, I., Ahmed, M.U., Winterbottom, F.L., von Scheven, G., Dietrich, S., 2007.
802 Extrinsic versus intrinsic cues in avian paraxial mesoderm patterning and differentiation.
803 *Dev Dyn* 236, 2397-2409.

- 804 Boyd, T.G., Castelli, W.A., Huelke, D.F., 1967. Removal of the temporalis muscle from
805 its origin: effects on the size and shape of the coronoid process. *Journal of dental*
806 *research* 46, 997-1001.
- 807 Brent, A.E., Braun, T., Tabin, C.J., 2005. Genetic analysis of interactions between the
808 somitic muscle, cartilage and tendon cell lineages during mouse development.
809 *Development* 132, 515-528.
- 810 Brent, A.E., Schweitzer, R., Tabin, C.J., 2003. A somitic compartment of tendon
811 progenitors. *Cell* 113, 235-248.
- 812 Brunt, L.H., Begg, K., Kague, E., Cross, S., Hammond, C.L., 2017. Wnt signalling
813 controls the response to mechanical loading during zebrafish joint development.
814 *Development* 144, 2798-2809.
- 815 Buxton, P.G., Hall, B., Archer, C.W., Francis-West, P., 2003. Secondary chondrocyte-
816 derived Ihh stimulates proliferation of periosteal cells during chick development.
817 *Development* 130, 4729-4739.
- 818 Callahan, J.F., Burgess, J.L., Fornwald, J.A., Gaster, L.M., Harling, J.D., Harrington,
819 F.P., Heer, J., Kwon, C., Lehr, R., Mathur, A., Olson, B.A., Weinstock, J., Laping, N.J.,
820 2002. Identification of novel inhibitors of the transforming growth factor beta1 (TGF-
821 beta1) type 1 receptor (ALK5). *J Med Chem* 45, 999-1001.
- 822 Carter, D.R., Beaupré, G.S., 2007. *Skeletal Function and Form: Mechanobiology of*
823 *Skeletal Development, Aging, and Regeneration*. Cambridge University Press.
- 824 Dawson, M.M., Metzger, K.A., Baier, D.B., Brainerd, E.L., 2011. Kinematics of the
825 quadrate bone during feeding in mallard ducks. *Journal of Experimental Biology* 214,
826 2036-2046.
- 827 del Rio, A., Perez-Jimenez, R., Liu, R.C., Roca-Cusachs, P., Fernandez, J.M., Sheetz,
828 M.P., 2009. Stretching Single Talin Rod Molecules Activates Vinculin Binding. *Science*
829 323, 638-641.
- 830 Dupont, S., Morsut, L., Aragona, M., Enzo, E., Giulitti, S., Cordenosi, M., Zanconato,
831 F., Le Digabel, J., Forcato, M., Bicciato, S., Elvassore, N., Piccolo, S., 2011. Role of
832 YAP/TAZ in mechanotransduction. *Nature* 474, 179-U212.
- 833 Ealba, E.L., Jheon, A.H., Hall, J., Curantz, C., Butcher, K.D., Schneider, R.A., 2015.
834 Neural crest-mediated bone resorption is a determinant of species-specific jaw length.
835 *Developmental biology* 408, 151-163.
- 836 Ealba, E.L., Schneider, R.A., 2013. A simple PCR-based strategy for estimating
837 species-specific contributions in chimeras and xenografts. *Development* 140, 3062-
838 3068.

- 839 Eames, B.F., Schneider, R.A., 2008. The genesis of cartilage size and shape during
840 development and evolution. *Development* 135, 3947-3958.
- 841 Edom-Vovard, F., Bonnin, M., Duprez, D., 2001. Fgf8 transcripts are located in tendons
842 during embryonic chick limb development. *Mech Dev* 108, 203-206.
- 843 Edom-Vovard, F., Schuler, B., Bonnin, M.A., Teillet, M.A., Duprez, D., 2002. Fgf4
844 positively regulates scleraxis and tenascin expression in chick limb tendons.
845 *Developmental biology* 247, 351-366.
- 846 Eichele, G., Tickle, C., Alberts, B.M., 1984. Microcontrolled release of biologically active
847 compounds in chick embryos: beads of 200-microns diameter for the local release of
848 retinoids. *Analytical biochemistry* 142, 542-555.
- 849 Eloy-Trinquet, S., Wang, H., Edom-Vovard, F., Duprez, D., 2009. Fgf signaling
850 components are associated with muscles and tendons during limb development. *Dev*
851 *Dyn* 238, 1195-1206.
- 852 Evans, D.J., Noden, D.M., 2006. Spatial relations between avian craniofacial neural
853 crest and paraxial mesoderm cells. *Dev Dyn* 235, 1310-1325.
- 854 Fang, J., Hall, B.K., 1997. Chondrogenic cell differentiation from membrane bone
855 periosteal. *Anat Embryol (Berl)* 196, 349-362.
- 856 Ferguson, C.M., Miclau, T., Hu, D., Alpern, E., Helms, J.A., 1998. Common molecular
857 pathways in skeletal morphogenesis and repair. *Ann N Y Acad Sci* 857, 33-42.
- 858 Fish, J.L., Schneider, R.A., 2014a. Assessing species-specific contributions to
859 craniofacial development using quail-duck chimeras. *J Vis Exp*.
- 860 Fish, J.L., Schneider, R.A., 2014b. Chapter 6 - Neural Crest-Mediated Tissue
861 Interactions During Craniofacial Development: The Origins of Species-Specific Pattern,
862 in: Trainor, P.A. (Ed.), *Neural Crest Cells*. Academic Press, Boston, pp. 101-124.
- 863 Fish, J.L., Sklar, R.S., Woronowicz, K.C., Schneider, R.A., 2014. Multiple
864 developmental mechanisms regulate species-specific jaw size. *Development* 141, 674-
865 684.
- 866 Grenier, J., Teillet, M.A., Grifone, R., Kelly, R.G., Duprez, D., 2009. Relationship
867 between neural crest cells and cranial mesoderm during head muscle development.
868 *PLoS One* 4, e4381.
- 869 Hall, B.K., 1967. The formation of adventitious cartilage by membrane bones under the
870 influence of mechanical stimulation applied in vitro. *Life Sciences* 6, 663-667.
- 871 Hall, B.K., 1968. In Vitro Studies on Mechanical Evocation of Adventitious Cartilage in
872 Chick. *Journal of Experimental Zoology* 168, 283-&.

- 873 Hall, B.K., 1972. Immobilization and Cartilage Transformation into Bone in Embryonic
874 Chick. *Anat Rec* 173, 391-&.
- 875 Hall, B.K., 1979. Selective proliferation and accumulation of chondroprogenitor cells as
876 the mode of action of biomechanical factors during secondary chondrogenesis.
877 *Teratology* 20, 81-91.
- 878 Hall, B.K., 1986. The Role of Movement and Tissue Interactions in the Development
879 and Growth of Bone and Secondary Cartilage in the Clavicle of the Embryonic Chick. *J*
880 *Embryol Exp Morph* 93, 133-152.
- 881 Hall, B.K., 2005. *Bones and cartilage : developmental and evolutionary skeletal biology*.
882 Elsevier Academic Press, San Diego, Calif.
- 883 Hall, B.K., Herring, S.W., 1990. Paralysis and Growth of the Musculoskeletal System in
884 the Embryonic Chick. *J Morphol* 206, 45-56.
- 885 Hall, J., Jheon, A.H., Ealba, E.L., Eames, B.F., Butcher, K.D., Mak, S.S., Ladher, R.,
886 Alliston, T., Schneider, R.A., 2014. Evolution of a developmental mechanism: Species-
887 specific regulation of the cell cycle and the timing of events during craniofacial
888 osteogenesis. *Developmental biology* 385, 380-395.
- 889 Hamburger, V., Balaban, M., Oppenheim, R., Wenger, E., 1965. Periodic motility of
890 normal and spinal chick embryos between 8 and 17 days of incubation. *J Exp Zool* 159,
891 1-13.
- 892 Hamill, O.P., McBride, D.W., 1996. The pharmacology of mechanogated membrane ion
893 channels. *Pharmacological Reviews* 48, 231-252.
- 894 Havis, E., Bonnin, M.A., Esteves de Lima, J., Charvet, B., Milet, C., Duprez, D., 2016.
895 TGFbeta and FGF promote tendon progenitor fate and act downstream of muscle
896 contraction to regulate tendon differentiation during chick limb development.
897 *Development* 143, 3839-3851.
- 898 Havis, E., Bonnin, M.A., Olivera-Martinez, I., Nazaret, N., Ruggiu, M., Weibel, J.,
899 Durand, C., Guerquin, M.J., Bonod-Bidaud, C., Ruggiero, F., Schweitzer, R., Duprez,
900 D., 2014. Transcriptomic analysis of mouse limb tendon cells during development.
901 *Development* 141, 3683-3696.
- 902 Hayamizu, T.F., Sessions, S.K., Wanek, N., Bryant, S.V., 1991. Effects of localized
903 application of transforming growth factor beta 1 on developing chick limbs.
904 *Developmental biology* 145, 164-173.
- 905 Horowitz, S.L., Shapiro, H.H., 1951. Modifications of mandibular architecture following
906 removal of temporalis muscle in the rat. *Journal of dental research* 30, 276-280.
- 907 Huang, A.H., Riordan, T.J., Pryce, B., Weibel, J.L., Watson, S.S., Long, F., Lefebvre, V.,
908 Harfe, B.D., Stadler, H.S., Akiyama, H., Tufa, S.F., Keene, D.R., Schweitzer, R., 2015.

- 909 Musculoskeletal integration at the wrist underlies the modular development of limb
910 tendons. *Development* 142, 2431-2441.
- 911 Huang, B., Takahashi, K., Sakata-Goto, T., Kiso, H., Togo, Y., Saito, K., Tsukamoto, H.,
912 Sugai, M., Akira, S., Shimizu, A., Bessho, K., 2013. Phenotypes of CCAAT/enhancer-
913 binding protein beta deficiency: hyperdantia and elongated coronoid process. *Oral*
914 *diseases* 19, 144-150.
- 915 Inman, G.J., Nicolas, F.J., Callahan, J.F., Harling, J.D., Gaster, L.M., Reith, A.D.,
916 Laping, N.J., Hill, C.S., 2002. SB-431542 is a potent and specific inhibitor of
917 transforming growth factor-beta superfamily type I activin receptor-like kinase (ALK)
918 receptors ALK4, ALK5, and ALK7. *Mol Pharmacol* 62, 65-74.
- 919 Kantomaa, T., Rönning, O., 1997. Growth Mechanisms of the Mandible, in: Dixon, A.D.,
920 Hoyte, D.A.N., Rönning, O. (Eds.), *Fundamentals of craniofacial growth*. CRC Press,
921 Boca Raton, pp. 189-204.
- 922 Kardon, G., 1998. Muscle and tendon morphogenesis in the avian hind limb.
923 *Development* 125, 4019-4032.
- 924 Kardon, G., Harfe, B.D., Tabin, C.J., 2003. A Tcf4-positive mesodermal population
925 provides a prepattern for vertebrate limb muscle patterning. *Dev Cell* 5, 937-944.
- 926 Kawarada, Y., Inoue, Y., Kawasaki, F., Fukuura, K., Sato, K., Tanaka, T., Itoh, Y.,
927 Hayashi, H., 2016. TGF-beta induces p53/Smads complex formation in the PAI-1
928 promoter to activate transcription. *Sci Rep-Uk* 6.
- 929 Kleinnulend, J., Roelofsen, J., Sterck, J.G.H., Semeins, C.M., Burger, E.H., 1995.
930 Mechanical Loading Stimulates the Release of Transforming Growth-Factor-Beta
931 Activity by Cultured Mouse Calvariae and Periosteal Cells. *J Cell Physiol* 163, 115-119.
- 932 Koo, B.S., Song, Y., Lee, S., Sung, Y.K., Sung, I.H., Jun, J.B., 2017. Prevalence and
933 distribution of sesamoid bones and accessory ossicles of the foot as determined by
934 digital tomosynthesis. *Clin Anat*.
- 935 Landmesser, L., Morris, D.G., 1975. The development of functional innervation in the
936 hind limb of the chick embryo. *J Physiol* 249, 301-326.
- 937 Livak, K.J., Schmittgen, T.D., 2001. Analysis of relative gene expression data using
938 real-time quantitative PCR and the 2(-Delta Delta C(T)) Method. *Methods* 25, 402-408.
- 939 Maeda, T., Sakabe, T., Sunaga, A., Sakai, K., Rivera, A.L., Keene, D.R., Sasaki, T.,
940 Stavnezer, E., Iannotti, J., Schweitzer, R., Ilic, D., Baskaran, H., Sakai, T., 2011.
941 Conversion of Mechanical Force into TGF-beta-Mediated Biochemical Signals. *Curr Biol*
942 21, 933-941.
- 943 Mammoto, T., Ingber, D.E., 2010. Mechanical control of tissue and organ development.
944 *Development* 137, 1407-1420.

- 945 Mathew, S.J., Hansen, J.M., Merrell, A.J., Murphy, M.M., Lawson, J.A., Hutcheson,
946 D.A., Hansen, M.S., Angus-Hill, M., Kardon, G., 2011. Connective tissue fibroblasts and
947 Tcf4 regulate myogenesis. *Development* 138, 371-384.
- 948 Matthews, B.D., Overby, D.R., Mannix, R., Ingber, D.E., 2006. Cellular adaptation to
949 mechanical stress: role of integrins, Rho, cytoskeletal tension and mechanosensitive ion
950 channels. *J Cell Sci* 119, 508-518.
- 951 McBeath, R., Pirone, D.M., Nelson, C.M., Bhadriraju, K., Chen, C.S., 2004. Cell shape,
952 cytoskeletal tension, and RhoA regulate stem cell lineage commitment. *Developmental*
953 *Cell* 6, 483-495.
- 954 Merrill, A.E., Eames, B.F., Weston, S.J., Heath, T., Schneider, R.A., 2008.
955 Mesenchyme-dependent BMP signaling directs the timing of mandibular osteogenesis.
956 *Development* 135, 1223-1234.
- 957 Moore, W.J., 1973. An experimental study of the functional components of growth in the
958 rat mandible. *Acta anatomica* 85, 378-385.
- 959 Moore, W.J., 1981. *The Mammalian Skull*. Cambridge University Press, Cambridge.
- 960 Moss, M.L., Meehan, M.A., 1970. Functional cranial analysis of the coronoid process in
961 the rat. *Acta anatomica* 77, 11-24.
- 962 Murakami, S., Kan, M., McKeehan, W.L., de Crombrughe, B., 2000. Up-regulation of
963 the chondrogenic Sox9 gene by fibroblast growth factors is mediated by the mitogen-
964 activated protein kinase pathway. *P Natl Acad Sci USA* 97, 1113-1118.
- 965 Murchison, N.D., Price, B.A., Conner, D.A., Keene, D.R., Olson, E.N., Tabin, C.J.,
966 Schweitzer, R., 2007. Regulation of tendon differentiation by scleraxis distinguishes
967 force-transmitting tendons from muscle-anchoring tendons. *Development* 134, 2697-
968 2708.
- 969 Naderi, J., Bernreuther, C., Grabinski, N., Putman, C.T., Henkel, B., Bell, G., Glatzel,
970 M., Sultan, K.R., 2009. Plasminogen activator inhibitor type 1 up-regulation is
971 associated with skeletal muscle atrophy and associated fibrosis. *Am J Pathol* 175, 763-
972 771.
- 973 Nguyen, J., Tang, S.Y., Nguyen, D., Alliston, T., 2013. Load Regulates Bone Formation
974 and Sclerostin Expression through a TGF beta-Dependent Mechanism. *Plos One* 8.
- 975 Niswander, L., Tickle, C., Vogel, A., Booth, I., Martin, G.R., 1993. FGF-4 replaces the
976 apical ectodermal ridge and directs outgrowth and patterning of the limb. *Cell* 75, 579-
977 587.
- 978 Noden, D., Schneider, R.A., 2006. Neural Crest Cells and the Community of Plan for
979 Craniofacial Development: Historical Debates and Current Perspectives, in: Saint-

- 980 Jeannet, J.-P. (Ed.), Neural crest induction and differentiation. Landes Bioscience,
981 Georgetown, Tex., pp. 1-23.
- 982 Noden, D.M., 1983. The Role of the Neural Crest in Patterning of Avian Cranial
983 Skeletal, Connective, and Muscle Tissues. *Developmental biology* 96, 144-165.
- 984 Noden, D.M., 1988. Interactions and fates of avian craniofacial mesenchyme.
985 *Development* 103, 121-140.
- 986 Noden, D.M., Trainor, P.A., 2005. Relations and interactions between cranial mesoderm
987 and neural crest populations. *J Anat* 207, 575-601.
- 988 Oka, K., Oka, S., Hosokawa, R., Bringas, P., Brockhoff, H.C., Nonaka, K., Chai, Y.,
989 2008. TGF-beta mediated Dlx5 signaling plays a crucial role in osteo-chondroprogenitor
990 cell lineage determination during mandible development. *Developmental biology* 321,
991 303-309.
- 992 Oka, K., Oka, S., Sasaki, T., Ito, Y., Bringas, P., Nonaka, K., Chai, Y., 2007. The role of
993 TGF-beta signaling in regulating chondrogenesis and osteogenesis during mandibular
994 development. *Developmental biology* 303, 391-404.
- 995 Ornitz, D.M., Marie, P.J., 2015. Fibroblast growth factor signaling in skeletal
996 development and disease. *Genes Dev* 29, 1463-1486.
- 997 Pitsillides, A.A., 2006. Early effects of embryonic movement: 'a shot out of the dark'.
998 *Journal of Anatomy* 208, 417-431.
- 999 Pollard, A.S., McGonnell, I.M., Pitsillides, A.A., 2014. Mechanoadaptation of developing
1000 limbs: shaking a leg. *Journal of Anatomy* 224, 615-623.
- 1001 Presnell, J.K., Schreiber, M.P., 1997. *Humason's Animal Tissue Techniques*. Johns
1002 Hopkins University Press.
- 1003 Pruitt, B.L., Dunn, A.R., Weis, W.I., Nelson, W.J., 2014. Mechano-Transduction: From
1004 Molecules to Tissues. *Plos Biol* 12.
- 1005 Pryce, B.A., Watson, S.S., Murchison, N.D., Staverosky, J.A., Duker, N., Schweitzer, R.,
1006 2009. Recruitment and maintenance of tendon progenitors by TGF beta signaling are
1007 essential for tendon formation. *Development* 136, 1351-1361.
- 1008 Quinn, T.P., Schlueter, M., Soifer, S.J., Gutierrez, J.A., 2002. Mechanotransduction in
1009 the lung - Cyclic mechanical stretch induces VEGF and FGF-2 expression in pulmonary
1010 vascular smooth muscle cells. *Am J Physiol-Lung C* 282, L897-L903.
- 1011 Raizman, I., De Croos, J.N., Pilliar, R., Kandel, R.A., 2010. Calcium regulates cyclic
1012 compression-induced early changes in chondrocytes during in vitro cartilage tissue
1013 formation. *Cell calcium* 48, 232-242.

- 1014 Ramage, L., Nuki, G., Salter, D.M., 2009. Signalling cascades in mechanotransduction:
1015 cell-matrix interactions and mechanical loading. *Scandinavian Journal of Medicine &*
1016 *Science in Sports* 19, 457-469.
- 1017 Rinon, A., Lazar, S., Marshall, H., Buchmann-Moller, S., Neufeld, A., Elhanany-Tamir,
1018 H., Taketo, M.M., Sommer, L., Krumlauf, R., Tzahor, E., 2007. Cranial neural crest cells
1019 regulate head muscle patterning and differentiation during vertebrate embryogenesis.
1020 *Development* 134, 3065-3075.
- 1021 Robbins, J.R., Evanko, S.P., Vogel, K.G., 1997. Mechanical loading and TGF-beta
1022 regulate proteoglycan synthesis in tendon. *Arch Biochem Biophys* 342, 203-211.
- 1023 Roberts, S.R., Knight, M.M., Lee, D.A., Bader, D.L., 2001. Mechanical compression
1024 influences intracellular Ca(2+) signaling in chondrocytes seeded in agarose constructs.
1025 *J Appl Physiol* 90, 1385-1391.
- 1026 Robling, A.G., Kang, K.S., Bullock, W.A., Foster, W.H., Muruges, D., Loots, G.G.,
1027 Genetos, D.C., 2016. Sost, independent of the non-coding enhancer ECR5, is required
1028 for bone mechanoadaptation. *Bone* 92, 180-188.
- 1029 Robling, A.G., Niziolek, P.J., Baldrige, L.A., Condon, K.W., Allen, M.R., Alam, I.,
1030 Mantila, S.M., Gluhak-Heinrich, J., Bellido, T.M., Harris, S.E., Turner, C.H., 2008.
1031 Mechanical stimulation of bone in vivo reduces osteocyte expression of Sost/sclerostin.
1032 *J Biol Chem* 283, 5866-5875.
- 1033 Rolfe, R.A., Nowlan, N.C., Kenny, E.M., Cormican, P., Morris, D.W., Prendergast, P.J.,
1034 Kelly, D., Murphy, P., 2014. Identification of mechanosensitive genes during skeletal
1035 development: alteration of genes associated with cytoskeletal rearrangement and cell
1036 signalling pathways. *BMC Genomics* 15, 48.
- 1037 Rot-Nikcevic, I., Downing, K.J., Hall, B.K., Kablar, B., 2007. Development of the mouse
1038 mandibles and clavicles in the absence of skeletal myogenesis. *Histology and*
1039 *histopathology* 22, 51-60.
- 1040 Russell, E.S., 1916. *Form and Function: A Contribution to the History of Animal*
1041 *Morphology*. John Murray Publishers Ltd., London.
- 1042 Sanford, L.P., Ormsby, I., GittenbergerdeGroot, A.C., Sariola, H., Friedman, R., Boivin,
1043 G.P., Cardell, E.L., Doetschman, T., 1997. TGF beta 2 knockout mice have multiple
1044 developmental defects that are nonoverlapping with other TGF beta knockout
1045 phenotypes. *Development* 124, 2659-2670.
- 1046 Schneider, R.A., 1999. Neural crest can form cartilages normally derived from
1047 mesoderm during development of the avian head skeleton. *Developmental biology* 208,
1048 441-455.
- 1049 Schneider, R.A., 2005. Developmental mechanisms facilitating the evolution of bills and
1050 quills. *J Anat* 207, 563-573.

- 1051 Schneider, R.A., 2007. How to tweak a beak: molecular techniques for studying the
1052 evolution of size and shape in Darwin's finches and other birds. *Bioessays* 29, 1-6.
- 1053 Schneider, R.A., 2015. Regulation of Jaw Length During Development, Disease, and
1054 Evolution. *Curr Top Dev Biol* 115, 271-298.
- 1055 Schneider, R.A., Helms, J.A., 2003. The cellular and molecular origins of beak
1056 morphology. *Science* 299, 565-568.
- 1057 Schneider, R.A., Hu, D., Rubenstein, J.L., Maden, M., Helms, J.A., 2001. Local retinoid
1058 signaling coordinates forebrain and facial morphogenesis by maintaining FGF8 and
1059 SHH. *Development* 128, 2755-2767.
- 1060 Schweitzer, R., Chyung, J.H., Murtaugh, L.C., Brent, A.E., Rosen, V., Olson, E.N.,
1061 Lassar, A., Tabin, C.J., 2001. Analysis of the tendon cell fate using Scleraxis, a specific
1062 marker for tendons and ligaments. *Development* 128, 3855-3866.
- 1063 Schweitzer, R., Zelzer, E., Volk, T., 2010. Connecting muscles to tendons: tendons and
1064 musculoskeletal development in flies and vertebrates (vol 137, pg 2807, 2010).
1065 *Development* 137, Ee47-Ee47.
- 1066 Shakibaei, M., Mobasheri, A., 2003. Beta1-integrins co-localize with Na, K-ATPase,
1067 epithelial sodium channels (ENaC) and voltage activated calcium channels (VACC) in
1068 mechanoreceptor complexes of mouse limb-bud chondrocytes. *Histology and*
1069 *histopathology* 18, 343-351.
- 1070 Sharir, A., Stern, T., Rot, C., Shahar, R., Zelzer, E., 2011. Muscle force regulates bone
1071 shaping for optimal load-bearing capacity during embryogenesis. *Development* 138,
1072 3247-3259.
- 1073 Shi, M., Zhu, J., Wang, R., Chen, X., Mi, L., Walz, T., Springer, T.A., 2011. Latent TGF-
1074 beta structure and activation. *Nature* 474, 343-349.
- 1075 Shibata, S., Suda, N., Fukada, K., Ohyama, K., Yamashita, Y., Hammond, V.E., 2003.
1076 Mandibular coronoid process in parathyroid hormone-related protein-deficient mice
1077 shows ectopic cartilage formation accompanied by abnormal bone modeling. *Anat*
1078 *Embryol (Berl)* 207, 35-44.
- 1079 Shwartz, Y., Blitz, E., Zelzer, E., 2013. One load to rule them all: mechanical control of
1080 the musculoskeletal system in development and aging. *Differentiation* 86, 104-111.
- 1081 Shwartz, Y., Farkas, Z., Stern, T., Aszodi, A., Zelzer, E., 2012. Muscle contraction
1082 controls skeletal morphogenesis through regulation of chondrocyte convergent
1083 extension. *Developmental biology* 370, 154-163.
- 1084 Smith, T.G., Sweetman, D., Patterson, M., Keyse, S.M., Munsterberg, A., 2005.
1085 Feedback interactions between MKP3 and ERK MAP kinase control scleraxis

- 1086 expression and the specification of rib progenitors in the developing chick somite.
1087 Development 132, 1305-1314.
- 1088 Solem, R.C., Eames, B.F., Tokita, M., Schneider, R.A., 2011. Mesenchymal and
1089 mechanical mechanisms of secondary cartilage induction. Developmental biology 356,
1090 28-39.
- 1091 Soni, N.N., Malloy, R.B., 1974. Effect of removal of the temporal muscle on the coronoid
1092 process in guinea pigs: quantitative triple fluorochrome study. Journal of dental research
1093 53, 474-480.
- 1094 Stutzmann, J., Petrovic, A., 1975. Nature and evolutive aptitudes of cells of the mitotic
1095 compartment of the secondary cartilages of the mandible and maxilla of the young rat.
1096 Experience with cytotypic culture and homotransplantation. Bulletin de l'Association des
1097 anatomistes 59, 523-534.
- 1098 Subramanian, A., Schilling, T.F., 2015. Tendon development and musculoskeletal
1099 assembly: emerging roles for the extracellular matrix. Development 142, 4191-4204.
- 1100 Sugimoto, Y., Takimoto, A., Akiyama, H., Kist, R., Scherer, G., Nakamura, T., Hiraki, Y.,
1101 Shukunami, C., 2013. Scx+/Sox9+ progenitors contribute to the establishment of the
1102 junction between cartilage and tendon/ligament. Development 140, 2280-2288.
- 1103 Sun, L., Tran, N., Liang, C., Tang, F., Rice, A., Schreck, R., Waltz, K., Shawver, L.K.,
1104 McMahon, G., Tang, C., 1999. Design, synthesis, and evaluations of substituted 3-[(3-
1105 or 4-carboxyethylpyrrol-2-yl)methylidene]indolin-2-ones as inhibitors of VEGF, FGF,
1106 and PDGF receptor tyrosine kinases. J Med Chem 42, 5120-5130.
- 1107 Sun, L., Tran, N., Tang, F., App, H., Hirth, P., McMahon, G., Tang, C., 1998. Synthesis
1108 and biological evaluations of 3-substituted indolin-2-ones: a novel class of tyrosine
1109 kinase inhibitors that exhibit selectivity toward particular receptor tyrosine kinases. J
1110 Med Chem 41, 2588-2603.
- 1111 Tanck, E., Blankevoort, L., Haaijman, A., Burger, E.H., Huijkes, R., 2000. Influence of
1112 muscular activity on local mineralization patterns in metatarsals of the embryonic
1113 mouse. J Orthop Res 18, 613-619.
- 1114 Thompson, D.W., 1942. On growth and form. On growth and form.
- 1115 Tokita, M., Schneider, R.A., 2009. Developmental origins of species-specific muscle
1116 pattern. Developmental biology 331, 311-325.
- 1117 Tu, X.L., Rhee, Y., Condon, K.W., Bivi, N., Allen, M.R., Dwyer, D., Stolina, M., Turner,
1118 C.H., Robling, A.G., Plotkin, L.I., Bellido, T., 2012. Sost downregulation and local Wnt
1119 signaling are required for the osteogenic response to mechanical loading. Bone 50,
1120 209-217.

- 1121 Tucker, A.S., Lumsden, A., 2004. Neural crest cells provide species-specific patterning
1122 information in the developing branchial skeleton. *Evol Dev* 6, 32-40.
- 1123 Vincent, T., Hermansson, M., Bolton, M., Wait, R., Saklatvala, J., 2002. Basic FGF
1124 mediates an immediate response of articular cartilage to mechanical injury. *P Natl Acad*
1125 *Sci USA* 99, 8259-8264.
- 1126 Vincent, T.L., McLean, C.J., Full, L.E., Peston, D., Saklatvala, J., 2007. FGF-2 is bound
1127 to perlecan in the pericellular matrix of articular cartilage, where it acts as a chondrocyte
1128 mechanotransducer. *Osteoarthritis Cartilage* 15, 752-763.
- 1129 Vinkka, H., 1982. Secondary cartilages in the facial skeleton of the rat. Proceedings of
1130 the Finnish Dental Society. Suomen Hammaslaakariseuran toimituksia 78 Suppl 7, 1-
1131 137.
- 1132 Wang, N., Tytell, J.D., Ingber, D.E., 2009. Mechanotransduction at a distance:
1133 mechanically coupling the extracellular matrix with the nucleus. *Nat Rev Mol Cell Bio*
1134 10, 75-82.
- 1135 Washburn, S.L., 1947. The relation of the temporal muscle to the form of the skull. *Anat*
1136 *Rec* 99, 239-248.
- 1137 Wassersug, R.J., 1976. A procedure for differential staining of cartilage and bone in
1138 whole formalin-fixed vertebrates. *Stain Technol* 51, 131-134.
- 1139 Wen, J., Tao, H., Lau, K., Liu, H., Simmons, C.A., Sun, Y., Hopyan, S., 2017. Cell and
1140 Tissue Scale Forces Coregulate Fgfr2-Dependent Tetrads and Rosettes in the Mouse
1141 Embryo. *Biophys J* 112, 2209-2218.
- 1142 Wipff, P.J., Rifkin, D.B., Meister, J.J., Hinz, B., 2007. Myofibroblast contraction activates
1143 latent TGF-beta1 from the extracellular matrix. *J Cell Biol* 179, 1311-1323.
- 1144 Wu, K.C., Streicher, J., Lee, M.L., Hall, B.K., Muller, G.B., 2001. Role of motility in
1145 embryonic development I: Embryo movements and amnion contractions in the chick
1146 and the influence of illumination. *Journal of Experimental Zoology* 291, 186-194.
- 1147 Zusi, R.L., 1993. Patterns of Diversity in the Avian Skull, in: Hanken, J., Hall, B.K.
1148 (Eds.), *The Skull*, First ed. University of Chicago Press, Chicago, pp. 391-437.
- 1149 Zweers, G., 1974. Structure, movement, and myography of the feeding apparatus of the
1150 mallard (*Anas platyrhynchos* L.). A study in functional anatomy. *Netherlands Journal of*
1151 *Zoology* 24(4), 323-467.
- 1152 Zweers, G.A., Kunz, G., Mos, J., 1977. Functional anatomy of the feeding apparatus of
1153 the mallard (*Anas platyrhynchos* L.) structure, movement, electro-myography and
1154 electro-neurography. *Anat Anz* 142, 10-20.
1155

TABLE 1.

Spatial Localization of Gene Expression in HH33 Control Duck

Structure	Tissue Type		FGF Signaling Pathway					TGFβ Signaling Pathway			
			<i>Fgf4</i>	<i>Fgf8</i>	<i>Fgfr2</i>	<i>Fgfr3</i>	<i>Pea3</i>	<i>Tgfβ2</i>	<i>Tgfβ3</i>	<i>Tgfβr2</i>	<i>Smad3</i>
Meckel's Cartilage	Primary Cartilage	Perichondrium			X		X				
		Cartilage	X	X	X	X	X		X	X	X
Coronoid Process	Secondary Cartilage	Condensation	X	X	X		X	X	X	X	
Surangular	Bone	Condensation	X	X	X	X	X				
Mandibular Adductor	Muscle		X	X			X	X	X	X	
Muscle Insertion	Tendon		X	X			X	X	X	X	

Spatial Localization of Gene Expression in HH36 Control Duck

Structure	Tissue Type		FGF Signaling Pathway					TGFβ Signaling Pathway			
			<i>Fgf4</i>	<i>Fgf8</i>	<i>Fgfr2</i>	<i>Fgfr3</i>	<i>Pea3</i>	<i>Tgfβ2</i>	<i>Tgfβ3</i>	<i>Tgfβr2</i>	<i>Smad3</i>
Meckel's Cartilage	Primary Cartilage	Perichondrium	X		X	X	X	X	X		X
		Cartilage	X	X	X	X	X	X	X		X
Coronoid Process	Secondary Cartilage	Perichondrium		X				X	X		X
		Cartilage	X	X	X	X	X	X	X	X	X
Surangular	Bone	Periosteum	X	X	X	X	X	X	X		X
		Bone	X	X	X	X	X	X	X	X	X
Mandibular Adductor	Muscle		X	X	X	X	X	X	X		X
Muscle Insertion	Tendon		X	X	X	X	X	X	X		X

1. Strong *Fgfr2* expression throughout the perichondrium with isolated cells expressing *Pea3*
2. Strong *Fgfr3* expression throughout with isolated cells expressing *Fgf8* and *Pea3*
3. Strong *Fgfr2* expression throughout the surangular condensation with isolated *Pea3* expressing cells
4. *Fgf4* and *Pea3* expression appear strongest near muscle tips while *Tgfβ2* is strongly expressed throughout the muscle
5. Strong *Fgfr2* expression throughout while *Fgfr3* expression is spatially restricted to the center
6. *Fgfr2* and *Fgfr3* are expressed throughout bone, but periosteal expression is quite strong
7. *Smad3* expression strongest near muscle insertions

Fig.1. Species-Specific form of the jaw and role of NCM. (A,B) Ventral views of left mandibles reveal the smooth appearance in quail and laterally protruding CP in duck (dashed circle). (C,D) Left lateral views of cleared and stained skulls showing cartilage (blue) and bone (red). A secondary cartilage forms on the lateral surface of the surangular in duck but not in quail. (E) Chimeric “chuck” were produced by unilaterally transplanting small NCM grafts from the midbrain and hindbrain of a GFP-positive chick donor into a comparable position in a stage-matched duck-host. (F) Small GFP-chick transplants yield a limited distribution of NCM-derived connective tissues. (G,H) The chick-donor side shows little transformation and resembles the contralateral control duck side with secondary cartilage present. (I,J,K,L) Larger NCM grafts distribute GFP-positive cells more broadly and lead to a loss of secondary cartilage relative to the contralateral, duck-host side.

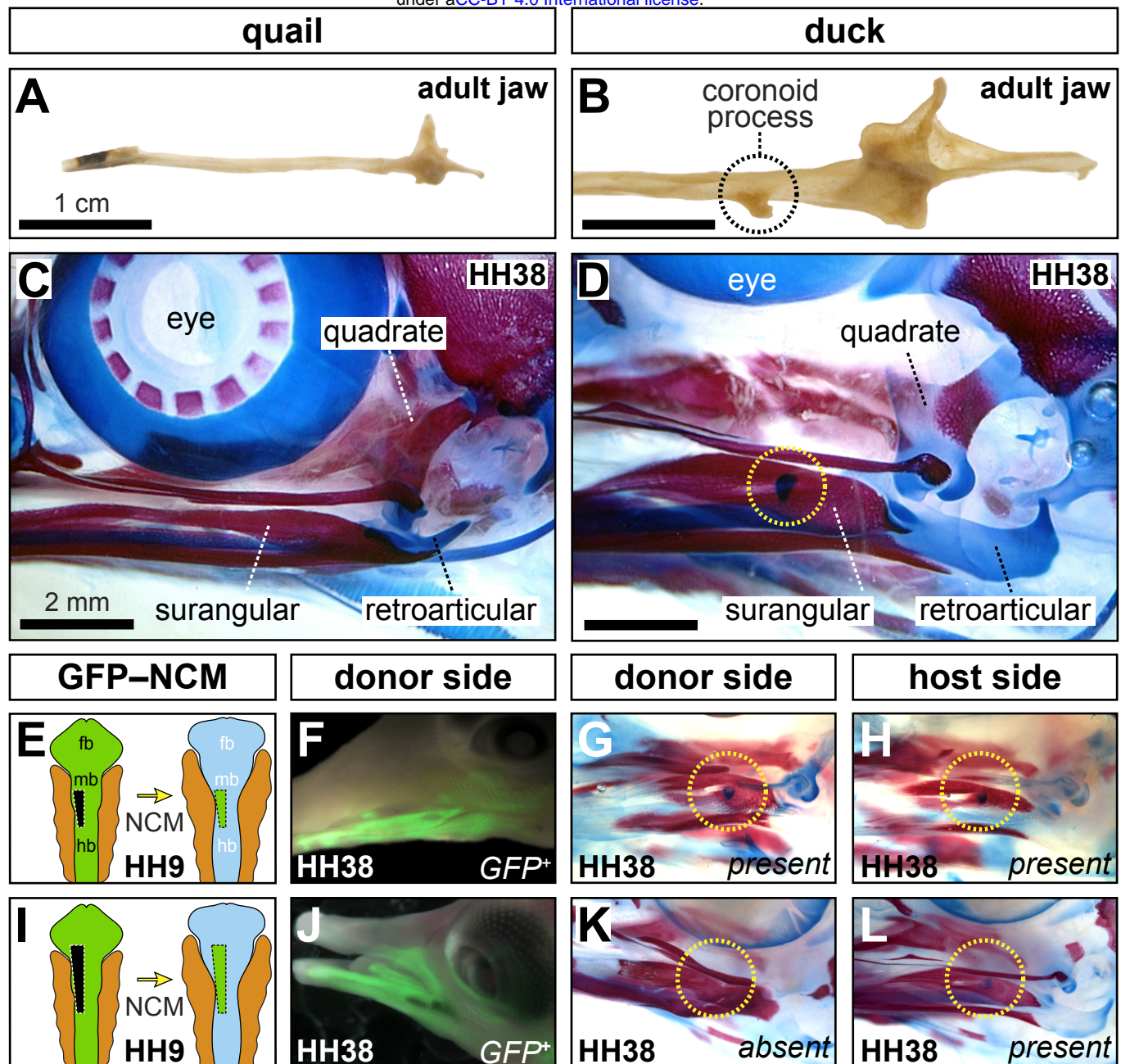
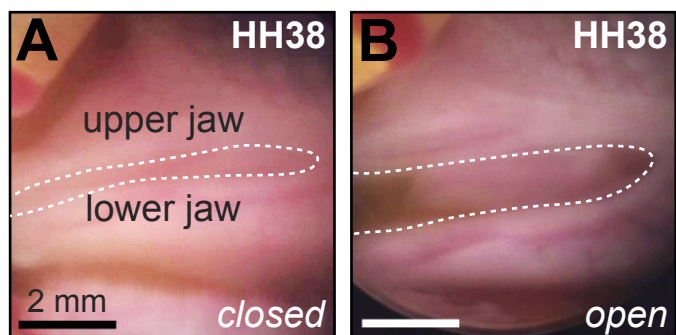
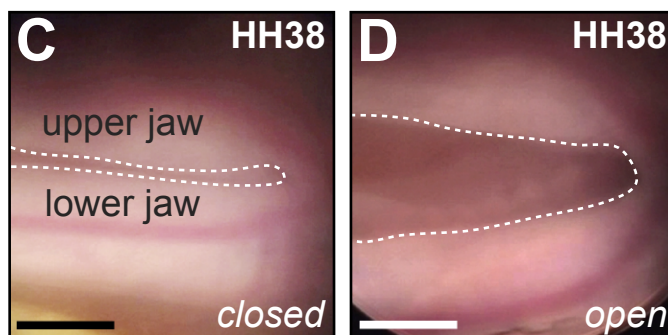


Fig.2. Jaw motility *in ovo*. (A,B,C,D) Representative open and closed jaw gaping positions in quail and duck embryos. (E) Actogram of 30-minute observation periods for representative quail and duck. Six consecutive stages were observed. Quail and duck activity periods steadily increase in frequency and duration. (F) During HH33, a key stage of secondary cartilage induction, the differences in jaw motility are minimal with quail being slightly more active, though the difference is not significant. Duck are significantly more active at HH36 ($p < 0.0005$).

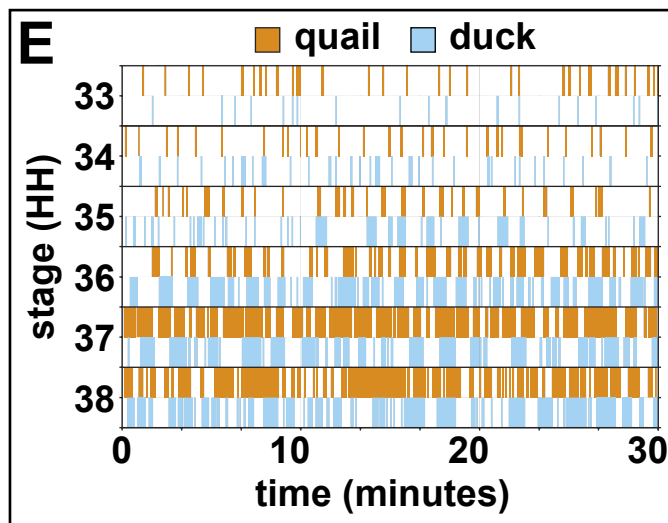
quail jaw gaping



duck jaw gaping



embryonic motility actogram



quail versus duck motility

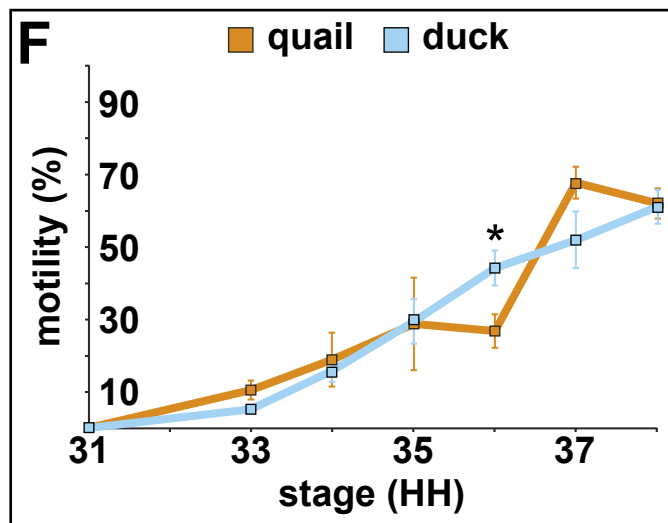
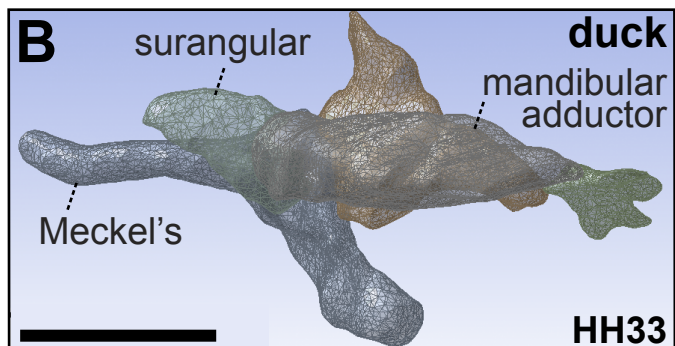
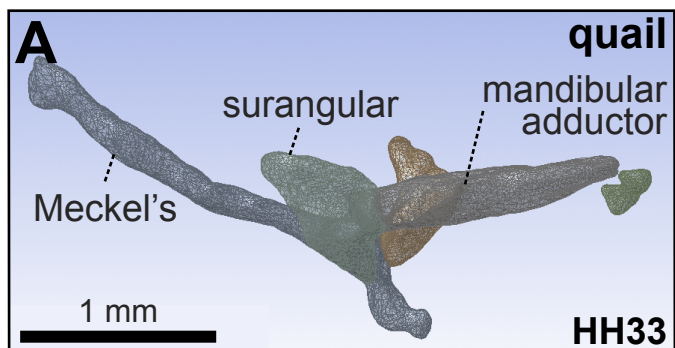


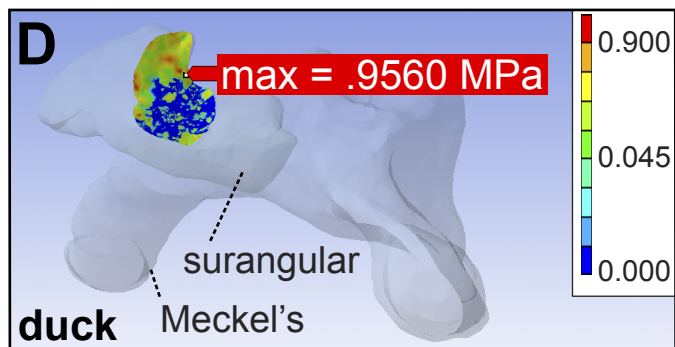
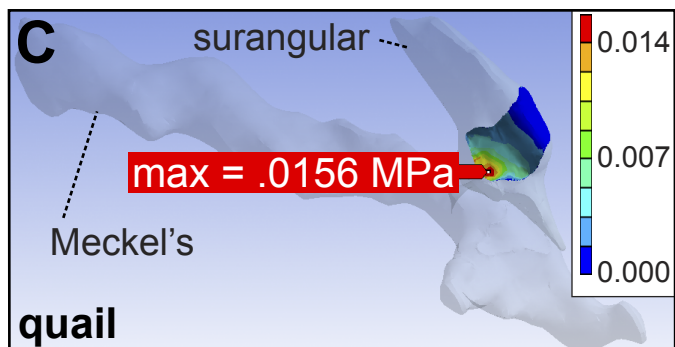
Fig.3. 3D reconstructions and finite element analysis of the adductor complex.

Three-dimensional wireframes of left **(A)** quail and **(B)** duck jaw showing the presumptive surangular (light-green), quadrate (red), MA muscle (purple), post-orbital (dark-green), and Meckel's (blue). Note the slender MA and its dorsal insertion on the quail surangular versus the bulky MA and its lateral insertion in duck. **(C)** Finite element modeling predicts a maximum von Mises stress concentration of 0.0156 MPa within the medial portion of the contact area between the MA and the surangular in quail. Color scales indicate predicted von Mises stress. **(D)** A maximum von Mises stress concentration of 0.9560 MPa is predicted within a dorsolateral region in duck. **(E)** Histogram of the range of von Mises stresses in duck versus quail. Note that the maximum von Mises stress in quail is substantially less than in duck.

three-dimensional wireframe



finite element analysis



von Mises stress distribution

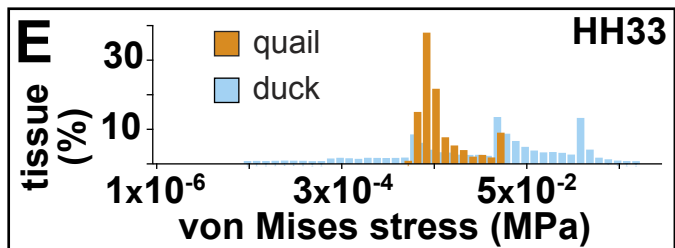


Fig.4. FGF pathway in paralyzed and control duck. (A) Differential expression in isolated MA entheses from HH33 and HH36 control and paralyzed embryos. Each gene is normalized to β -Actin and shown relative to HH33 controls. Error bars represent standard deviation. Asterisks denote statistical significance between control and paralyzed samples at HH36 (* $p < 0.05$; ** $p < 0.005$). (B) Sagittal section through the MA (ma) muscle insertion along the presumptive surangular (sa). A secondary cartilage condensation is present at the MA insertion on the CP (arrow). (C,D) *Fgf4* and *Fgfr2* (stained purple) are expressed in the secondary cartilage condensation and surrounding tissues. (E) *Fgfr3* is expressed around the margins of the surangular condensation. (F) 24 hours after paralysis at HH32, HH33 embryos show disrupted muscle and tendon, and there is no secondary cartilage condensation. (G,H) *Fgf4* and *Fgfr2* are altered and the secondary cartilage is absent. (I) *Fgfr3* is disrupted. (J) Sagittal section through the MA muscle insertion on the CP lateral to the surangular. The secondary cartilage (2°) is well formed. (K,L,M) *Fgf4*, *Fgfr2*, and *Fgfr3* are in the secondary cartilage and surrounding tissues. (N) Paralysis at HH32 prevents secondary cartilage formation (asterisk). The MA inserts directly onto the surangular. (O,P,Q) *Fgf4*, *Fgfr2*, and *Fgfr3* are altered and secondary cartilage is absent.

Changes in FGF pathway members in duck from HH33 to HH36

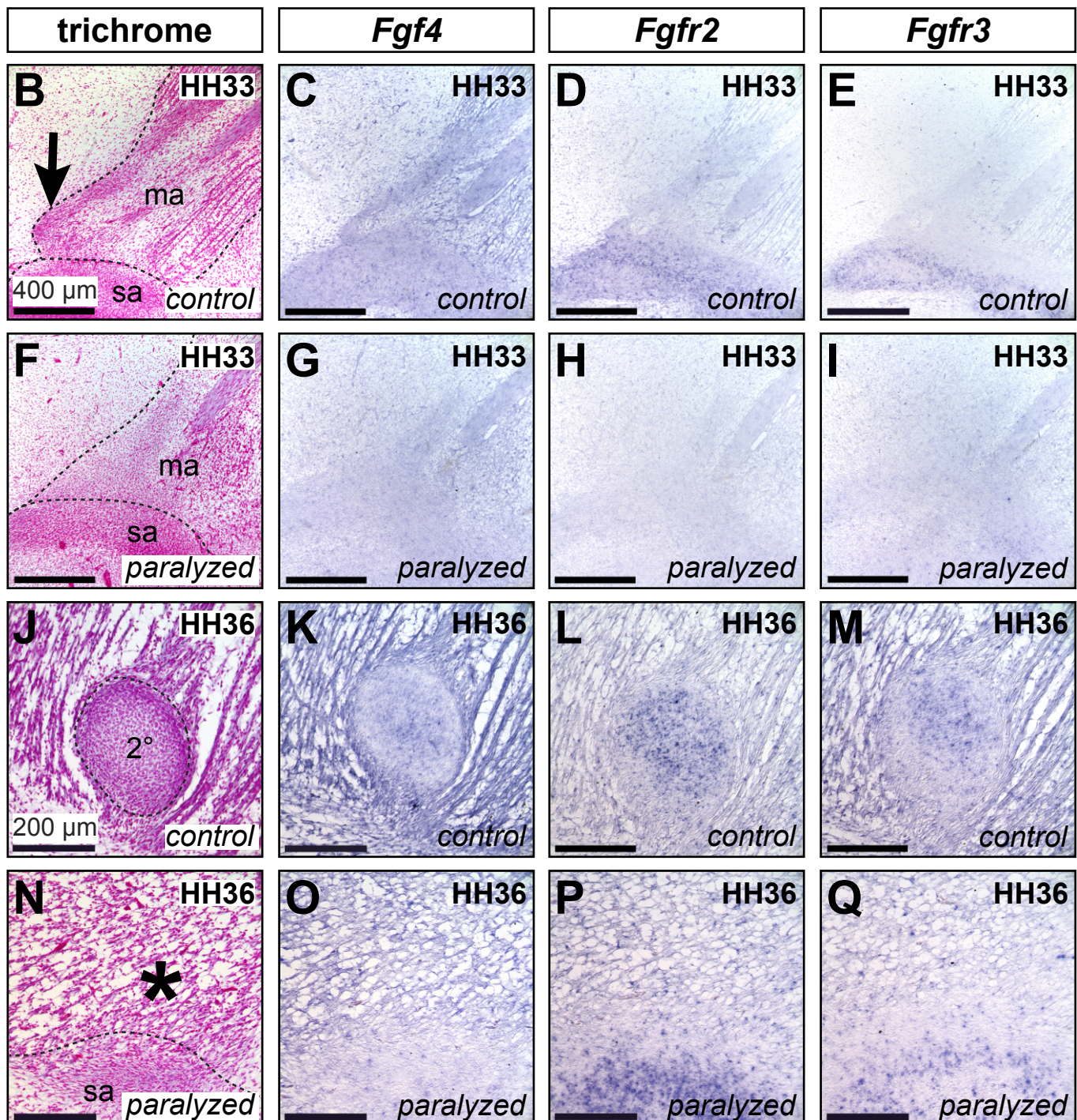
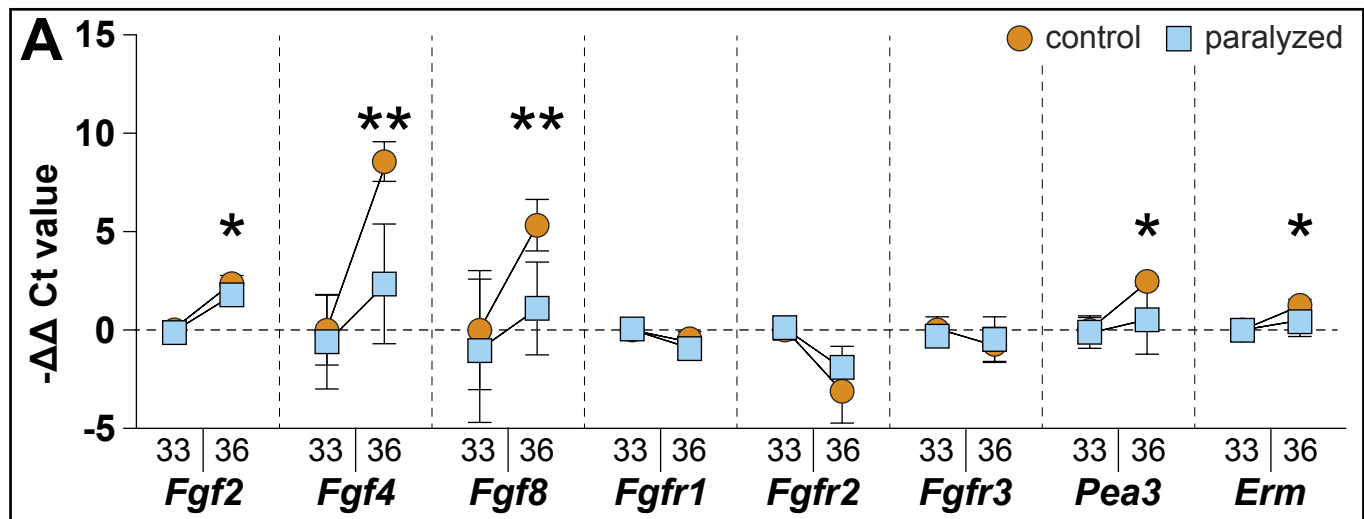


Fig.5. TGF β pathway in paralyzed and control duck. (A) Differential expression in isolated MA entheses from HH33 and HH36 control and paralyzed embryos. Each gene is normalized to *β -Actin* and displayed relative to HH33 controls. Error bars represent standard deviation. Asterisk denote statistical significance between control and paralyzed samples at HH36 (* $p < 0.05$). (B) Sagittal section through the MA (ma) muscle insertion along the presumptive surangular (sa). A secondary cartilage condensation is present at the MA insertion on the CP (arrow). (C,D,E) *Tgf β 2*, *Tgf β 3*, and *Tgf β r2* are expressed in the secondary cartilage condensation and surrounding tissues. (F) 24 hours after paralysis at HH32, HH33 embryos show disrupted muscle and tendon, and there is no secondary cartilage condensation. (G,H,I) *Tgf β 2*, *Tgf β 3*, and *Tgf β r2* are disrupted. There is no secondary cartilage condensation. (J) Sagittal section through the MA muscle insertion on the CP lateral to the surangular. The secondary cartilage (2°) is well formed. (K,L,M) *Tgf β 2*, *Tgf β 3*, and *Tgf β r2* are expressed in the secondary cartilage and surrounding tissues. (N) Paralysis at HH32 prevents secondary cartilage formation (asterisk). (O,P,Q) *Tgf β 2*, *Tgf β 3*, and *Tgf β r2* are altered and secondary cartilage is absent.

Changes in TGF β pathway members in duck from HH33 to HH36

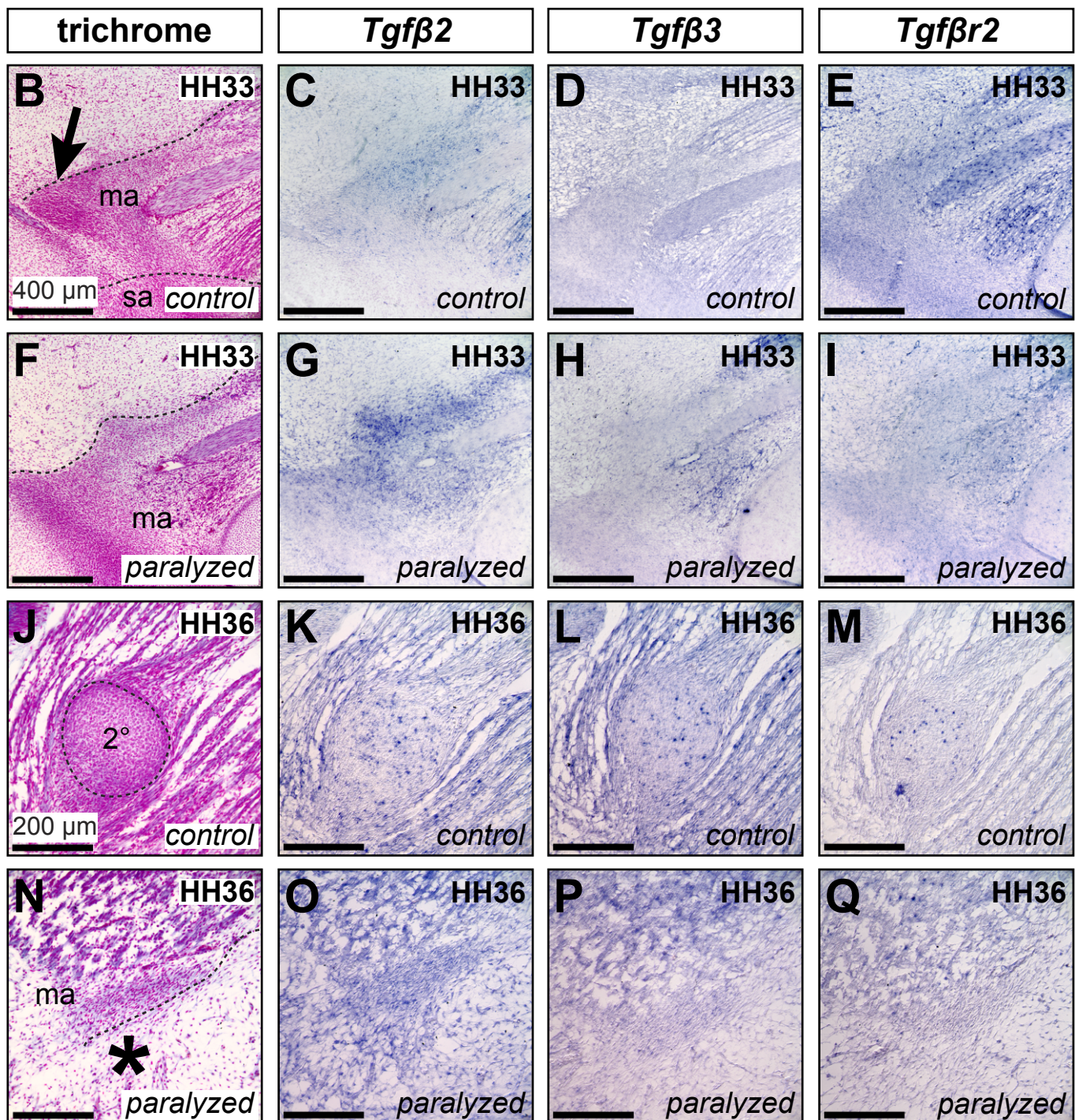
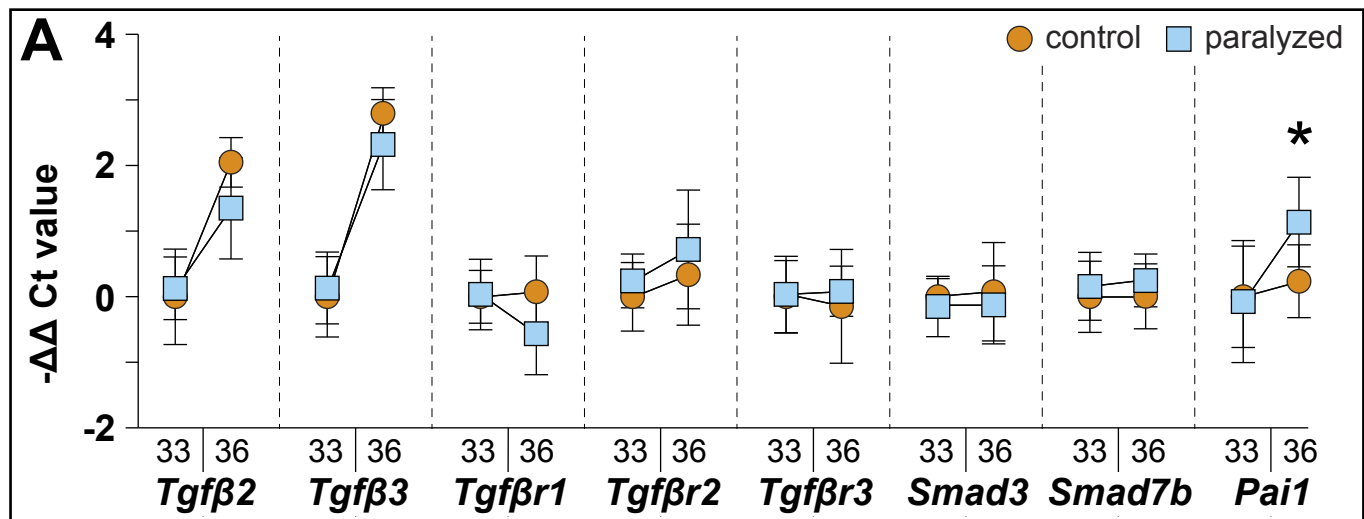
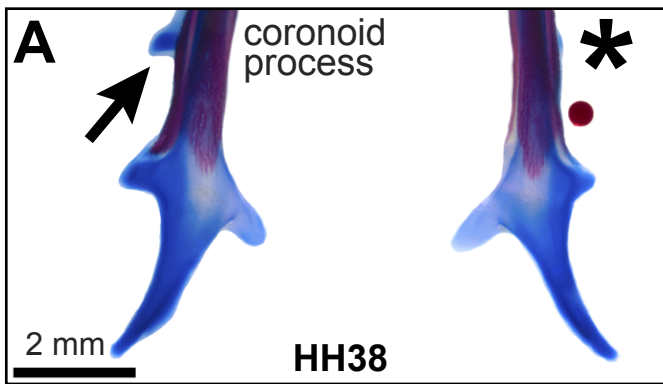


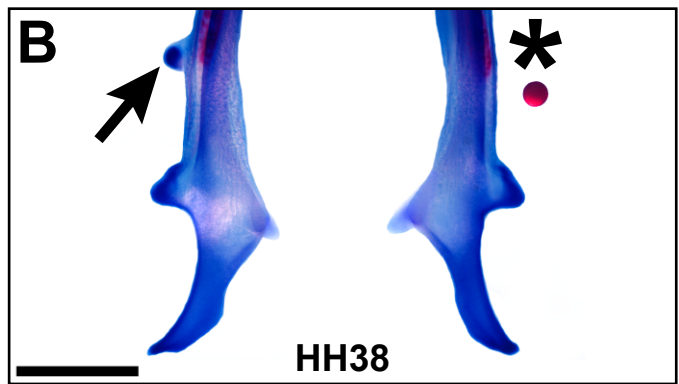
Fig.6. Inhibition of FGF and TGF β signaling during secondary chondrogenesis. (A)

Ventral view of a cleared and stained duck mandible treated with a bead soaked in an FGF inhibitor (SU5402). Note the loss of secondary cartilage (asterisk) while the untreated side develops normally (arrow). **(B)** Inhibition of TGF β signaling (SB431542) results in a loss of secondary cartilage while the control side develops normally. **(C)** FGF signaling inhibition eliminates or reduces secondary cartilage by HH38, with a greater treatment effect at HH32 versus HH33 (Fisher's Exact Test $p < 0.005$). **(D)** TGF β signaling inhibition eliminates or reduces secondary cartilage by HH38. **(E)** Inhibiting FGF or TGF β signaling does not increase apoptosis after 24 hours. Positive control, DNase digested slides displayed significant apoptosis (unpaired t-test $p < 0.0001$). **(F,G,H,I)** Sections from DMSO, SU5402, or SB431542 treated embryos reveal little apoptosis. Extensive positive staining was observed in DNase digested sections.

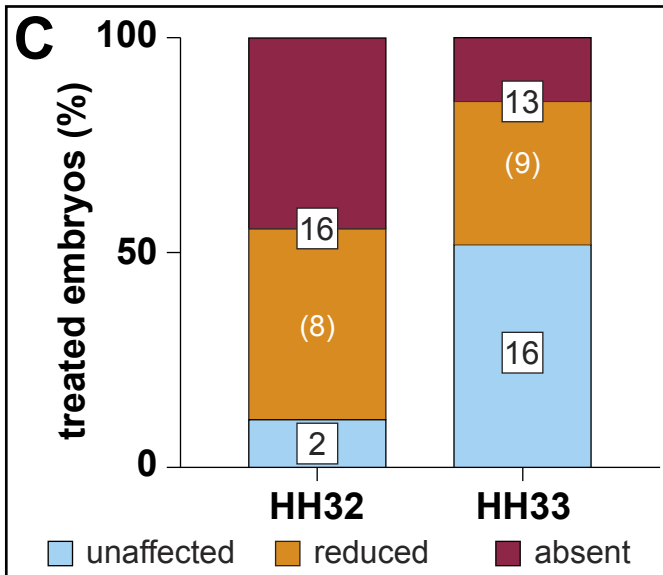
SU5402-treated duck at HH33



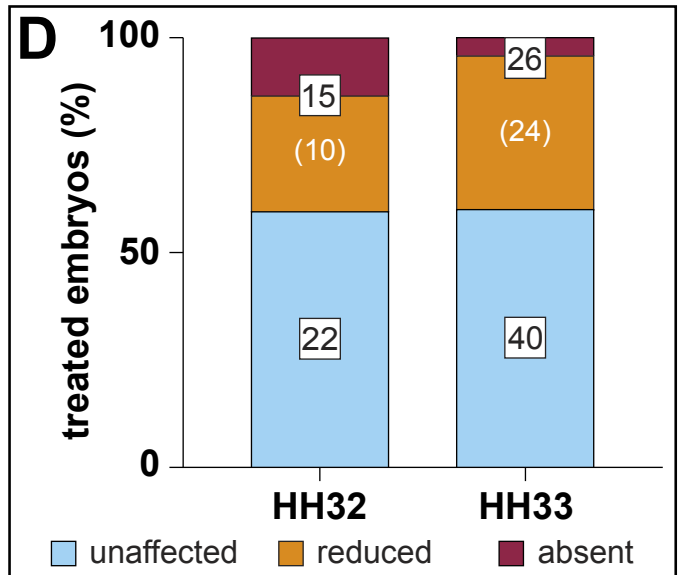
SB431542-treated duck at HH33



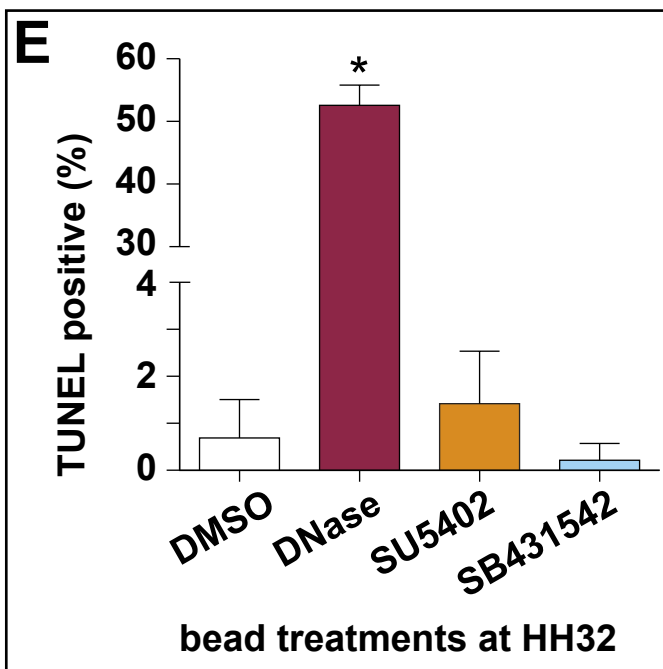
effects of SU5402



effects of SB431542



TUNEL analysis



TUNEL analysis

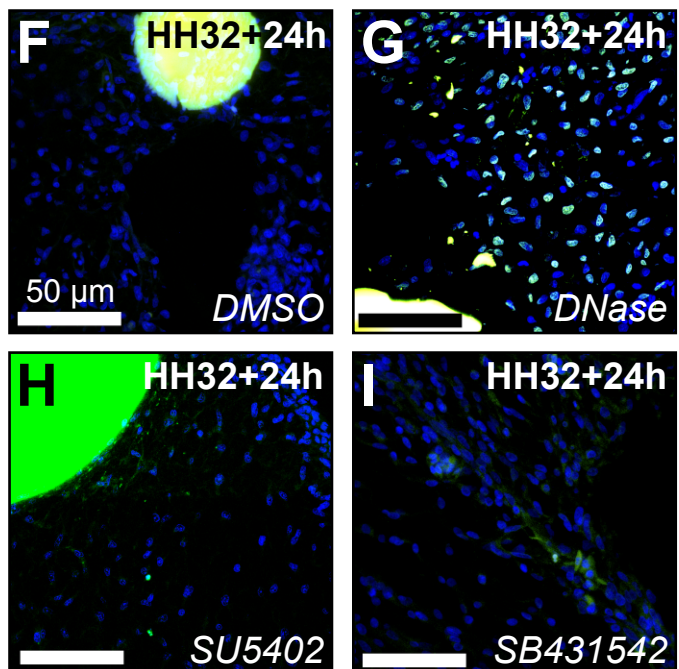


Fig.7. FGF4 and TGF β 2/TGF β 3 induce chondrogenesis. (A) Ventral view of a cleared and stained mandible treated with a BSA soaked bead. Carrier treatments exert no effect on secondary cartilage (asterisk). (B) HH32 FGF4 treatment induces cartilage (arrow) in paralyzed embryos by HH38. (C) TGF β 2/TGF β 3 treatment induces cartilage (arrow) in paralyzed embryos. (D) Combined FGF4 and TGF β 2/TGF β 3 treatments induce cartilage (arrow) despite paralysis. (E) HH38 sagittal section through the MA insertion of a paralyzed embryo implanted with FGF4 and TGF β 2/TGF β 3 beads at HH32. Safranin-O reveals dense, positively stained mesenchyme surrounding the beads (arrow). (F) HH32 TGF β 2/TGF β 3 treatment induces quail to form cartilage by HH38 (arrow). (G) FGF4, TGF β 2/TGF β 3, and FGF4/TGF β 2/TGF β 3 treatments induce cartilage by HH38. The distribution of treatment outcomes depends upon the ligand or ligands embryos receive (Fisher's Exact Test p=0.005).

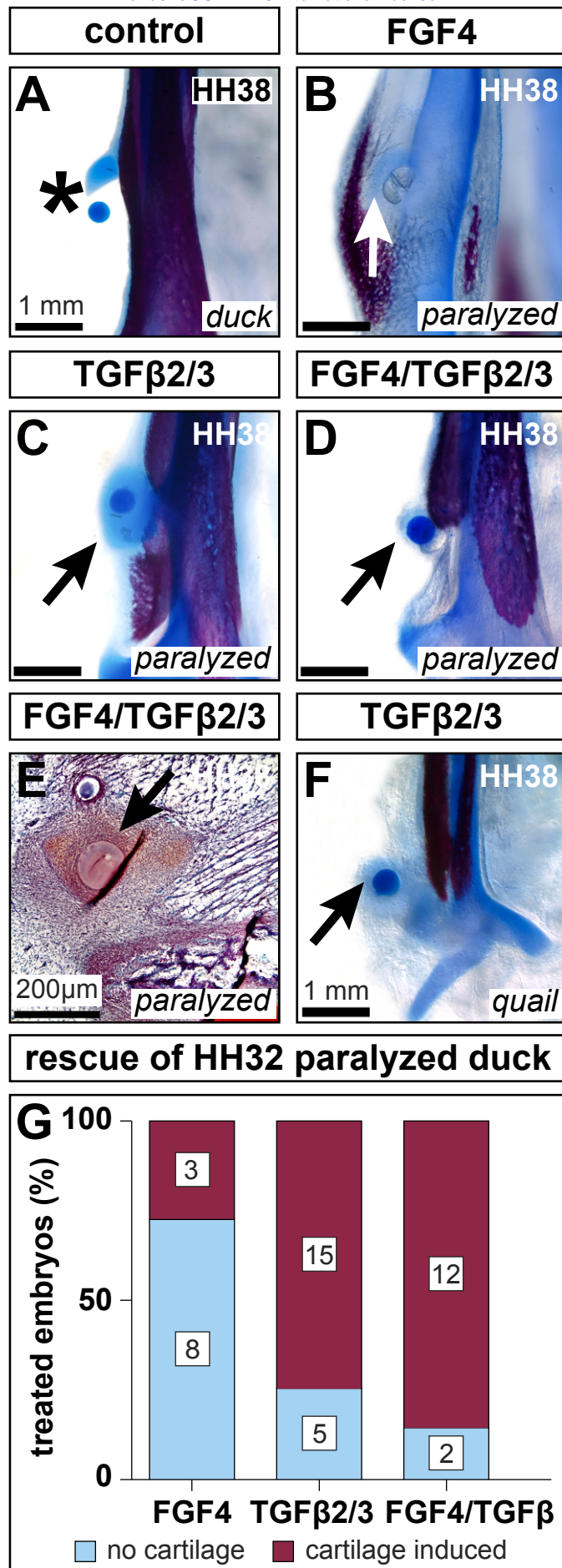


Fig.8. A model integrating form and function with FGF and TGF β signaling. NCM-mediated species-specific jaw geometry, (i.e., dorsal versus lateral MA insertions) and functional loading by embryonic motility contribute to differential forces and tissue differentiation. The resultant mechanical stress leads to differential activation of FGF and TGF β signaling and regulates the presence or absence of secondary cartilage on the CP. We observe three overlapping patterns of expression: One set is altered by growth (blue boxes), another altered by load (red boxes), and a third is altered by both growth and load (orange boxes). A fourth set of genes remains unaltered both during growth and despite a loss of embryonic motility (white boxes). Some genes are found in multiple sets, reflecting the complex integration of form and function during embryonic development.

A model for the relationship between form and function

